Measurements of ^{222}Rn, ^{220}Rn, and CO_2 Emissions in Natural CO_2 Fields in Wyoming: MVA Techniques for Determining Gas Transport and Caprock Integrity

Final Scientific/Technical Report

Reporting Period Start Date: January 1, 2010
Reporting Period End Date: September 30, 2014

Principal Author(s):
Dr. John P. Kaszuba
Dr. Kenneth W.W. Sims

Report Issued March 2015

DOE Award Number DE-FE0002112

University of Wyoming
Department of Geology and Geophysics
1000 E. University Ave. Dept. 3006
Laramie, WY 82071-2000

DISCLAIMER

ABSTRACT

An integrated field-laboratory program evaluated the use of radon and CO_2 flux measurements to constrain source and timescale of CO_2 fluxes in environments proximate to CO_2 storage reservoirs. By understanding the type and depth of the gas source, the integrity of a CO_2 storage reservoir can be assessed and monitored. The concept is based on correlations of radon and CO_2 fluxes observed in volcanic systems. This fundamental research is designed to advance the science of Monitoring, Verification, and Accounting (MVA) and to address the Carbon Storage Program goal of developing and validating technologies to ensure 99 percent storage performance. Graduate and undergraduate students conducted the research under the guidance of the Principal Investigators; in doing so they were provided with training opportunities in skills required for implementing and deploying CCS technologies.

Although a final method or "tool" was not developed, significant progress was made. The field program identified issues with measuring radon in environments rich in CO_2. Laboratory experiments determined a correction factor to apply to radon measurements made in CO_2-bearing environments. The field program also identified issues with radon and CO_2-flux measurements in soil gases at a natural CO_2 analog. A systematic survey of radon and CO_2 flux in soil gases at the LaBarge CO_2 Field in Southwest Wyoming indicates that measurements of ^{222}Rn (radon), ^{220}Rn (thoron), and CO_2 flux may not be a robust method for monitoring the integrity of a CO_2 storage reservoir. The field program was also not able to correlate radon and CO_2 flux in the CO_2-charged springs of the Thermopolis hydrothermal system. However, this part of the program helped to motivate the aforementioned laboratory experiments that determined correction factors for measuring radon in CO_2-rich environments. A graduate student earned a Master of Science degree for this part of the field program; she is currently employed with a geologic consulting company. Measurement of radon in springs has improved significantly since the field program first began; however, in situ measurement of ^{222}Rn and particularly ^{220}Rn in springs is problematic. Future refinements include simultaneous salinity measurements and systematic corrections, or adjustments to the partition coefficient as needed for more accurate radon concentration determination. A graduate student earned a Master of Science degree for this part of the field program; he is currently employed with a geologic consulting company. Both graduate students are poised to begin work in a CCS technology area.

Laboratory experiments evaluated important process-level fundamentals that effect measurements of radon and CO_2. Laboratory tests established that fine-grained source minerals yield higher radon emissivity compared to coarser-sized source minerals; subtleties in the dataset suggest that grain size alone is not fully representative of all the processes controlling the ability of radon to escape its mineral host. Emissivity for both ^{222}Rn and ^{220}Rn increases linearly with temperature due to reaction of rocks with water, consistent with faster diffusion and enhanced mineral dissolution at higher temperatures. The presence of CO_2 changes the relative importance of the factors that control release of radon. Emissivity for both ^{222}Rn and ^{220}Rn in CO_2-bearing experiments is greater at all temperatures compared to the experiments without CO_2, but emissivity does not increase as a simple function of temperature. Governing processes may include a balance between enhanced dissolution versus carbonate mineral formation in CO_2-rich waters.

TABLE OF CONTENTS

1. EXECUTIVE SUMMARY

This integrated field-laboratory program evaluated the use of radon and CO_2 flux measurements to constrain source and timescale of CO_2 fluxes in environments proximate to CO_2 storage reservoirs. By understanding the type and depth of the gas source, the integrity of a CO_2 storage reservoir can be assessed and monitored. The concept is based on correlations of radon and CO_2 fluxes observed in volcanic systems. This fundamental research is designed to advance the science of Monitoring, Verification, and Accounting (MVA) and to address the Carbon Storage Program goal of developing and validating technologies to ensure 99 percent storage performance. Graduate and undergraduate students conducted the research under the guidance of the Principal Investigators; in doing so they were provided with training opportunities in skills required for implementing and deploying CCS technologies.

The project consisted of the four tasks. 1) Evaluate utility of radon and CO_2-flux measurements in soil gases at a natural CO_2 analog. A systematic survey was conducted at the LaBarge CO_2 Field in Southwest Wyoming; 2) Develop methods and train students to make systematic measurements of radon and CO_2. We did this work at Yellowstone National Park where focused discharges of gases and waters contain measurable quantities of radon and CO_2. This work also afforded the opportunity to systematically evaluate potential correlations between dissolved CO_2 and Radon concentrations, and ($^{220}Rn/^{222}Rn$) activity ratios; 3) Evaluate these methods by making systematic measurements in a location where radon and CO_2 are likely to occur in measurable quantities. The measurements were conducted in Thermopolis, Wyoming, a non-volcanic setting where CO_2-charged waters are associated with actively upwelling CO_2; and 4) conduct laboratory tests to evaluate effects of the characteristics of mineralogic sources of Rn emissions and of geochemical reactions that take place in CO_2-rich environments

Although a final method or "tool" was not developed, significant progress was made. The field program identified issues with measuring radon in environments rich in CO_2. Laboratory experiments determined that when Rn is measured in the presence of CO_2 the ^{220}Rn measurement is diminished more than the ^{222}Rn reading and that therefore the $^{220}Rn/^{222}Rn$ decreases as a function of CO_2 concentration. Thus a correction factor was developed for use in field and laboratory environments where radon and CO_2 measurements are made. The field program also identified issues with radon and CO_2-flux measurements in soil gases at a natural CO_2 analog. A systematic survey of radon and CO_2 flux in soil gases at the LaBarge CO_2 Field in Southwest Wyoming indicates that Rn measurements could not be correlated to CO_2 flux. Our results indicate that measurements of ^{222}Rn, ^{220}Rn, and CO_2 flux may not be a robust method for monitoring the integrity of a CO_2 storage reservoir.

The field program was not able to correlate radon and CO_2 flux in the CO_2-charged springs of the Thermopolis hydrothermal system. However, this part of the program helped to motivate the laboratory experiments that determined correction factors for measuring radon in CO_2-rich environments. It produced the first geochemical analyses of the CO_2-charged springs of Thermopolis in over 30 years and evaluated the aqueous geochemistry of this system. It also provided a graduate student the opportunity to earn a Master of Science degree; this student is now gainfully employed with a geologic consulting company and is poised to begin work in a CCS technology area.

Measurement of radon and thoron in springs has improved significantly since the field program first began; however, in situ measurement of radon, and particularly thoron (^{220}Rn) in springs is problematic. Even duplicate measurements taken in the same location are not within error (while the CO_2, meanwhile, remained more or less constant). The possible cause(s) of these variations is not readily apparent. Temporal variations in radon flux and dissolved radon concentrations, even on the timescale of minutes to hours, may be a significant source of radon variation. Despite the fact that radon is non-reactive, changes in water chemistry may still influence radon exsolution. Future refinements include simultaneous salinity measurements and systematic corrections, or adjustments to the partition coefficient as needed for more accurate radon concentration determination. This part of the program provided a second graduate student the opportunity to earn a Master of Science degree; this student is now gainfully employed with a geologic consulting company and is poised to begin work in a CCS technology area.

Laboratory experiments evaluated important process-level fundamentals that effect measurements of radon and CO_2. As expected, the laboratory tests revealed that fine-grained source minerals yield higher radon emissivity compared to coarser-sized source minerals. However, subtleties in the dataset suggest that grain size alone is not fully representative of all the processes controlling the ability of radon to escape its mineral host. Also as expected, reaction of rocks with water indicate that emissivity for both ^{222}Rn and ^{220}Rn increases linearly with temperature. This is consistent with temperature-dependent diffusion from within the minerals and with enhanced mineral dissolution at higher temperatures. The presence of CO_2 changes the relative importance of the factors that control release of radon. Emissivity for both ^{222}Rn and ^{220}Rn in CO_2-bearing experiments is greater at all temperatures compared to the experiments without CO_2, but emissivity does not increase as a simple function of temperature. Governing processes may include a balance between enhanced dissolution versus carbonate mineral formation in CO_2-rich waters.

2. REPORT DETAILS

2.1 Introduction

2.1.1 Purpose

This project was completed as part of the DOE Geological Sequestration Training and Research Program. The purpose of the program was to advance the United States in its position as the leader in technology for addressing climate change and for developing near-zero emission technologies to significantly reduce CO_2 emissions from power plants. Two major objectives were identified in the Funding Opportunity Announcement (DE-FOA-0000032) for this program. First, to provide training opportunities for graduate and undergraduate students that will provide the human capital and skills required for implementing and deploying CCS technologies. This training was accomplished through fundamental research in a CCS technology area. Second, to make a vital contribution to the scientific, technical, and institutional knowledge necessary to establish frameworks for the development of commercial CCS projects.

In this final report we describe and summarize the results of our project in the context of these two objectives. Students who worked on this project were trained in fundamental aspects of geology and geochemistry to advance the technology area of monitoring, verification, and accounting. We first summarize the fundamental research conducted by these students and present findings and conclusions produced as a consequence of this work. We do not merely compile information contained in other reports; we provide information in an integrated fashion as drawn from the research as a whole. Where appropriate we refer the reader to our earlier reports where additional information and details can be found. We then identify these students, summarize their accomplishments, and (where possible) describe their current employment status.

2.1.2 Background

Carbon dioxide (CO_2) occurs naturally in the Earth's crust and is an important constituent in many volcanic and hydrothermal settings. Geologic reservoirs have naturally stored supercritical CO_2 for geologic scales of time; these are often referred to as natural analogs (Allis et al., 2001). These natural occurrences of CO_2 provide a means of understanding and predicting behavior in carbon repositories, particularly for investigating and improving technologies and protocols aimed at assessing the integrity of caprock formations. Wyoming is home to all of these different styles of naturally occurring CO_2. The Thermopolis, Wyoming hydrothermal system is the surface expression of actively upwelling CO_2; it includes hot springs, travertine deposits, and thermal wells along the Bighorn River in the southern portion of the Bighorn Basin of Wyoming (Figure 1). The Yellowstone Volcanic System contributes significantly to global volcanic CO_2 emissions (Werner et al., 2000). In Yellowstone, CO_2 is derived from magmatic degassing as well as hydrolysis or thermal breakdown of Paleozoic and Mesozoic sediments and is estimated at $3.7 \pm 1.3 \times 10^{11}$ mol y^{-1} or 45 ± 16 kt d^{-1} (Werner and Brantley, 2003). Finally, at least eight natural analogues are located in Wyoming (De Bruin, 1991; Allis et al., 2001; De Bruin et al., 2004) (Figure 1).

Radon (Rn) is a noble gas and the only naturally occurring radioactive gas. It has two isotopes, ^{222}Rn (Radon) and ^{220}Rn (Thoron), relevant to this project. For this report, we use "Radon" and "Rn" to denote the element and all its isotopes; we use ^{222}Rn and ^{220}Rn to denote the specific

isotope. ^{222}Rn is a short-lived decay product derived from the ^{238}U decay series, with a half-life of 3.82 days. ^{220}Rn is a decay product derived from the ^{232}Th decay series and has an even shorter half-life (56 seconds) that makes it useful in discriminating areas of very fast soil-gas transport. Elevated Rn emissions are grossly correlated with high CO_2 emissions in volcanic systems, thus, ^{222}Rn provides a means to identify deep CO_2 activity and map active, high porosity regions. Because of its short half-life, ^{222}Rn, possesses the unique advantage of being able to constrain timescales of CO_2 migration. However, because the main source of the measured Rn (shallow soil degassing, deep reservoir degassing or both) is undetermined, the nature and relevance of the temporal constraints from ^{222}Rn remain uncertain (Figure 2).

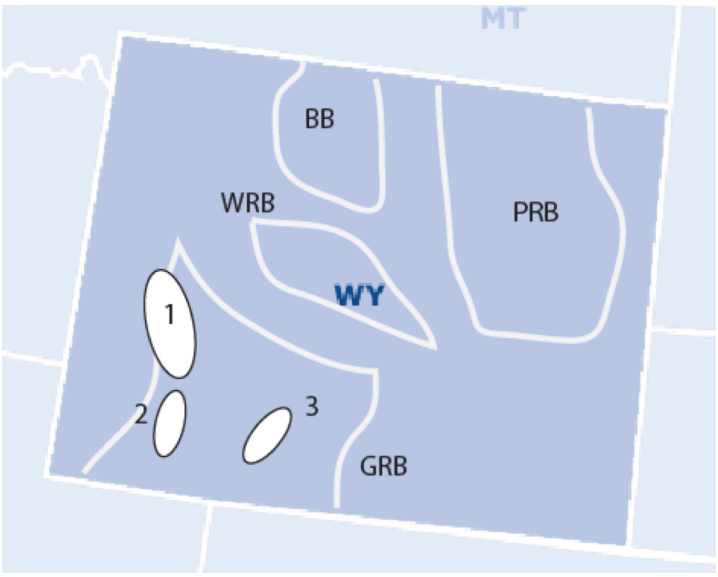

Figure 1. Location of natural CO_2 analogues in Wyoming that coincide with background gamma radiation anomalies (1 = La Barge; 2 = Bruff, Church Buttes, and Butcher Knife Springs; 3 = Brady). Schematic outlines of major Wyoming basins are also shown (BB = Bighorn Basin; PRB = Powder River Basin; WRB = Wind River Basin; GRB = Greater Green River Basin). Adapted from De Bruin (1991), Cannia and Case (1986), and De Bruin et al. (2004).

In volcanic systems, because of significant differences in their half-lifes, ^{220}Rn and ^{222}Rn activities and soil CO_2 flux appear to follow a general empirical relationship where the higher the flux of CO_2, the lower the ratio between ^{220}Rn and ^{220}Rn (Giammanco et al., 2007). Deep sources of gas are characterized by high ^{222}Rn activity and high CO_2 efflux, whereas shallow sources exhibit high ^{220}Rn activity and relatively low CO_2 flux. Deviations from this relationship reflect perturbations to the natural steady-state system. In volcanic systems excess ^{220}Rn highlights sites of ongoing shallow rock fracturing indicative of likely and imminent collapse (Giammanco, 2007). In anthropogenic carbon systems, such as CCS reservoirs, caprock leakage or failure may produce similar excesses of ^{220}Rn over the steady state ^{222}Rn/^{220}Rn. The ***scientific objective*** for this project was to evaluate relationships between ^{222}Rn/^{220}Rn and CO_2; this relationship may provide essential insight as to the type and depth of the gas source and, indirectly, the integrity of a CO_2 storage reservoir near sampling locations (Figure 2). This in turn supports the Carbon Storage Program goal to develop and validate technologies to ensure 99 percent storage performance. To reach this objective and provide ***training opportunities***, a diverse set of field and laboratory tasks was performed by four graduate and four undergraduate students; these students were mentored by the Principal Investigators.

2.1.3 Overview

The project consisted of the following four tasks.

1) Evaluate utility of radon and CO_2-flux measurements in soil gases at a natural CO_2 analog. At least five of the eight natural CO_2 analogs in Wyoming (Figure 1) coincide with areas of elevated gamma background radioactivity that may indicate potential Rn degassing (Cannia and Case, 1986; De Bruin, 1991; De Bruin et al., 2004). We conducted a systematic survey of radon and CO_2 flux in soil gases at one of these locations, the LaBarge CO_2 Field in Southwest Wyoming along the Moxa Arch (Figure 1).

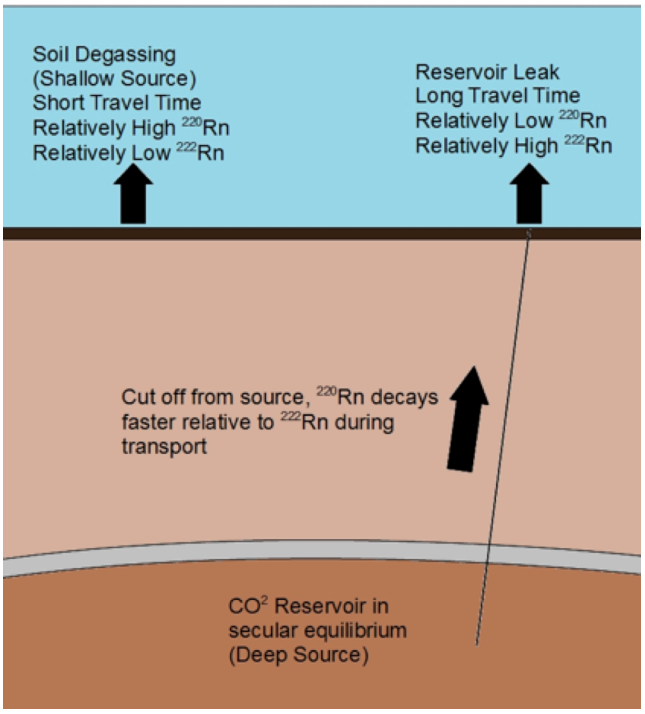

Figure 2. Conceptual diagram of difference in Radon values between two sources.

2) Develop methods and train students to make systematic measurements of Radon and CO_2. We chose locations that are characterized by focused discharges of gases and waters containing measurable quantities of Radon and CO_2. The measurements were conducted in Yellowstone National Park in the far northwest corner of Wyoming. This also afforded the opportunity to systematically evaluate potential correlations between dissolved CO_2 and Radon concentrations, and ($^{220}Rn/^{222}Rn$) activity ratios.

3) Evaluate the methods by making systematic measurements of Radon and CO_2 in a location where Radon and CO_2 are likely to occur in measurable quantities. The measurements were conducted in Thermopolis, Wyoming, in the southern edge of the Bighorn Basin (Figure 1). Thermopolis is a non-volcanic setting where CO_2-charged waters are associated with actively upwelling CO_2.

4) Evaluate effects of the characteristics of mineralogic sources of Rn emissions and of geochemical reactions that take place in CO_2-rich environments on Radon and CO_2 measurements. In order to use ^{220}Rn and ^{222}Rn as a monitoring tool, the behavior of Radon sources and the relation to geochemical and mineralogic properties must be understood. This evaluation was conducted in a controlled laboratory environment. Originally two sets of tests were to be performed. The first set was to evaluate measurable Radon activity as a function of surface area and surface:volume ratios of source geomaterials. The second set was to evaluate how CO_2-H_2O-rock reactions may influence measurable Radon activity by changing surface area (thus surface:volume ratios) and by armoring reactive surfaces of geomaterials. As the project evolved it became apparent that the influence of lithology also needed to be evaluated. Thus a third set of tests was added to the experimental program.

2.2 Methods

2.2.1 Radon Isotope Measurements

^{222}Rn (radon) and ^{220}Rn (thoron) are measured using a Durridge Inc. RAD7 radon-in-air monitor. Thus far we have successfully employed three different systems for measuring radon in water, all of these were purchased through Durridge Inc. they are: 1) RAD AQUA 2) Big Bottle H2O (Figure 3) 3) RAD H2O.

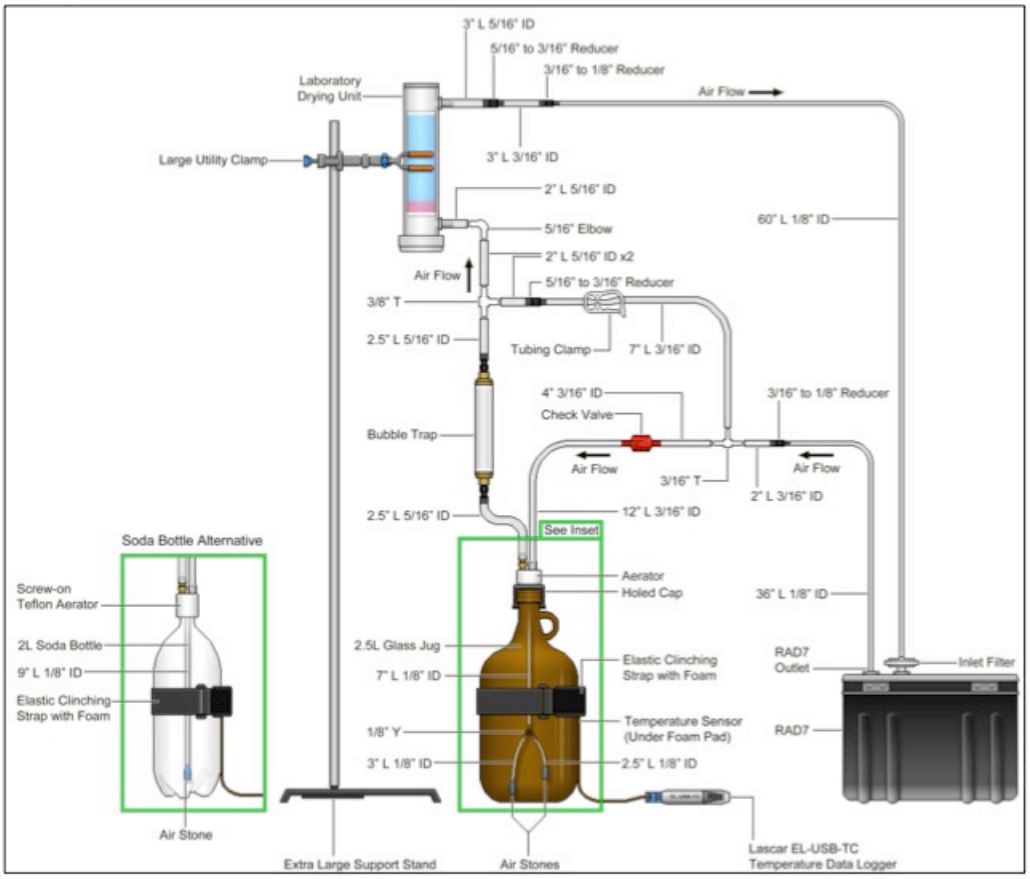

Figure 1. Big Bottle H2O Setup

In the case of the Big Bottle H2O and the RAD H2O, water is collected in pre-rinsed glass containers (2.5 L and 250 mL respectively) and connected to the RAD7 in a closed air loop. The water is aerated with airstones for 45 minutes (Big Bottle H2O) and five minutes (RAD H2O) in order to release the radon from the water and circulate the air in the closed loop until the loop has reached concentration equilibrium. The RAD7 counts the decays of radon and thoron via solid state α-detection. The data is downloaded to CAPTURE© where the activity of radon in water is calculated from the counts per minute of the radon daughters, the volume in the system, the temperature of the water (Big Bottle H2O only – a separate temperature data logger is employed during measurement) and the Rn – water partition coefficient. The lag time between sample collection and analysis is too long to retain measurable thoron ($t_{1/2}$ = 55s) for both the Big Bottle H2O and the RAD H2O – so only radon is measured using these two systems. Due to the small sample size (and therefore relatively poor counting statistics) the RAD H2O is only used occasionally, predominately when suspended sediment concentrations are too high to permit the

use of the RAD AQUA. The RAD H2O is then employed for comparison to Big Bottle H2O and for data redundancy.

The RAD AQUA (Figure 4 is an airtight water / gas exchanger cylinder. Water from hot springs is pumped to spray nozzles that effectively remove radon and thoron from the water where it is then pumped into a closed air loop with the RAD7.

The RAD AQUA provides the only reliable means with which to measure thoron because the "closed" loop to the RAD7 is circulating gas through the system from the constant influx of "fresh" water fast enough to circulate into the RAD7 scintillation chamber before decaying. A 0-100% CO_2 meter is placed just downstream of the RAD7 outlet which can simultaneously record CO_2 concentration in the closed air loop. A temperature probe attached to a temperature data logger is inserted into the RAD AQUA to accurately measure and record water temperature. Using optimal air and water flow rates into the RAD7 and RAD AQUA respectively, water / air equilibrium can be attained in 25-30 mins (Dimova et al., 2009) and the RAD7 can monitor temporal changes to radon and thoron concentrations. One important caveat of the RAD AQUA system is its incompatibility with significant amounts of sediment, large particulates, and or organic matter (algae, etc) that may be present in the water.

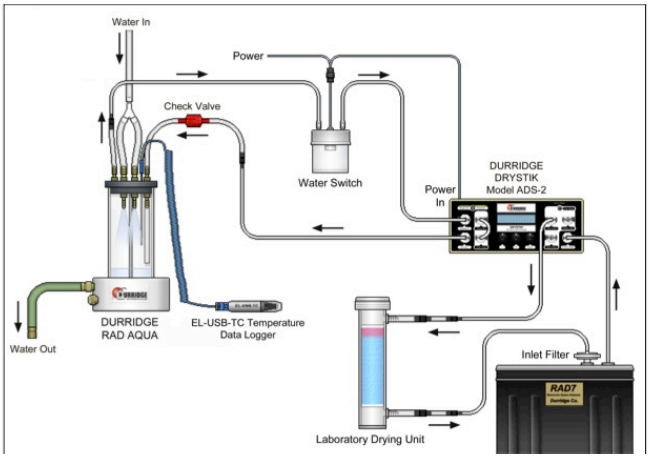

Figure 4. Diagram of the RAD AQUA setup

2.2.2 Rn and CO_2 Soil Flux Measurements

Here we summarize methods for Rn and CO_2 flux measurements employed for the field study of a natural CO_2 reservoir, the Moxa Arch of Southwest Wyoming. Details are provided in the Quarterly Progress Report for July-September, 2010. Carbon dioxide de-gassing was measured in the soil using the PP Systems (http://www.ppsystems.com/) EGM 4 Environmental Gas Monitor flux meter. The flux meter measures a rate of increase of CO_2 in a closed cylindrical chamber of a known volume with an open base that permits soil gas to enter. The chamber collects the soil gases in situ and calculates the flux rate CO_2/unit area/unit time (PP Systems, 2007). During the initial measurements of CO_2, the change of concentration is proportional to the efflux of CO_2 (Tonani, F. and G. Miele, 1991). The radon (^{222}Rn) and thoron (^{220}Rn) concentrations were determined using a Durridge RAD7.

Measurements are performed in areas of minimal vegetation. Vegetation that was present was removed along with the top one to two cm of soil. After the area was cleared, the sample was taken after ten or more minutes to allow for biogenic activity to dissipate achieving a more accurate measurement. The measurement is made by placing the chamber firmly on the ground, completely submerging the base in the soil to eliminate atmospheric gas from skewing the flux, and allow the flux meter to run. This measurement was repeated 3 to 5 times and the results were averaged.

2.2.3 Measurements of CO_2-Charged Water

CO_2 flux and radon activity from upwelling springs charged with CO_2 took place at the Thermopolis, Wyoming hydrothermal system. The methods employed in this early work are described in detail in the Quarterly Progress Reports for July-September 2010, October-December 2010, January-March 2011, April-June 2011, and in the Pluda (2012) MS thesis (Appendix 1, Sections 1.1, 1.2, and 1.3 (radon and thoron measurements) and Section 1.5 (CO_2 flux measurements)). As will be discussed in the Section 2.3.3, these early attempts yielded poor results and these methods will not be discussed further. However, these efforts helped lay the foundation for development of robust methods for measuring radon and thoron in CO_2-rich environments (Sections 2.2.1 and 2.3.1).

The regional and local geology of the Thermopolis, Wyoming hydrothermal system was also evaluated to provide context for understanding CO_2 flux from the upwelling springs. A quantitative assessment of the regional and local hydrogeochemistry was conducted as part of this evaluation. To develop a regional geochemical perspective, analyses of formation waters sampled from underlying formations were compiled for oil and gas fields proximate to the Thermopolis hydrothermal system. Historic analyses of the local springs dating back to 1906 were tabulated, and new geochemical data were developed by sampling the springs over the course of a year. Standard geologic and geochemical field and laboratory methods were employed to develop these datasets, further details are provided in the above-referenced Quarterly Progress Reports and in Pluda (2012) and Kaszuba et al. (2014).

2.2.4 Laboratory Methods

Laboratory experiments were performed to evaluate three important factors that could affect interaction of radon and thoron with CO_2: lithology of the source rock, surface area and surface:volume ratios of source minerals, and reaction of source rock with formation waters and CO_2. As discussed in Section 2.1.3, the experiments to evaluate lithology were not originally part of the workscope; as the project evolved these experiments were identified as essential and added to the experimental program.

Methods used to evaluate surface area, surface:volume ratios, and lithology. Laboratory methods for these tests were described in detail in the Quarterly Progress Report for October-December, 2013. To summarize, a total of nine experiments were performed. These tests evaluated size fractions of 4-6 mm, 0.85-1 mm, and 45-75 μm; surface area and surface:volume ratios are properties of the size of individual grains of mineral or rock. These tests also evaluated three different lithologies containing low, medium, and high concentrations of parent isotopes of radon: Banco Bonito Obsidian, Cerros Del Rio Basalt, and Guaje Pumice, respectively. Each of the nine samples was sealed in individual containers for 20 days to allow radon and thoron to equilibrate in the pore space. Activities of ^{222}Rn and ^{220}Rn were subsequently measured by connecting each container to a RAD7 via a closed loop system.

Methods used to evaluate reaction of source rock with formation waters and CO_2. The experiments were originally going to be performed using rocking autoclaves and flexible Au reaction cells (Kaszuba et al., 2003). However, in conducting the experiments to evaluate surface area, surface:volume ratios, and lithology, we identified practical constraints for making reliable measurements of ^{222}Rn and ^{220}Rn activities in this apparatus. Thus an alternate method

was developed and a different experimental apparatus used. Detailed descriptions and schematic drawings of the experimental setup were described in the Quarterly Progress Report for January-March, 2014. These design specifications are reproduced in Appendix A and summarized below.

A total of nine experiments were performed; experimental parameters are tabulated in Table 1. One size fraction of Cerros Del Rio Basalt (45-75μm) was reacted with water (designated as H_2O+Rock experiments) and with CO_2-charged water (designated as CO_2+H_2O+Rock experiments) in separate experiments. The NaCl and Na_2CO_3 concentrations for the experiments represent a reasonable salinity and CO_2 content for natural waters and CO_2+-waters, respectively. Initial experiments (not reported herein) were conducted at 21, 50, 90°C, temperatures that bracket a broad range of reservoir conditions. Technical difficulties with the 90°C experiments lead us to conduct subsequent experiments at 25, 40, and 60°C, temperatures that still represent a reasonable range of reservoir conditions.

Table 1. Experimental parameters for fluid-rock experiments

	Low Salinity H_2O+Rock Experiments	H_2O+Rock Experiments	CO_2+H_2O+Rock Experiments
Water chemistry	10 mmol/kg NaCl	28 mmol/kg NaCl	28 mmol/kg Na_2CO_3
Temperature	25, 40, 60°C		
Initial Water:Rock Ratio	10:1		
Duration	20 days		

Each experiment was housed in sealed 250 ml bottles containing 22.5 g rock, 225 g water, and approximately 15 cm^3 of headspace. Secular equilibrium was reached after 20 days. Each experiment was subsequently attached to a closed loop configuration; air was cycled through the system for 40 minutes to equilibrate ^{222}Rn and ^{220}Rn activities between air and water. Air from the closed loop was then cycled through the RAD7. The RAD7 was run twice for 12 hours per sample, once with the pump on for 4 minutes every 20 minutes to accurately measure ^{222}Rn activity and once with the pump on for the 12 hour duration to accurately measure ^{220}Rn activity. This experiment was repeated again but the RAD7 was run 3 times with the pump on the 20 minute cycle and 3 times with the pump on continuously (alternating between the two). The known volume of air and water allowed calculation of the ^{222}Rn and ^{220}Rn activities in both air and water.

2.3. Results and Discussion

2.3.1 Effect of CO_2 on RAD7 Radon Measurements

To investigate a CO_2 effect and evaluate whether the observed inverse relationship between $^{220}Rn/^{222}Rn$ and CO_2 is a true geochemical signal, or potentially an analytical artifact of high CO_2 concentrations, we conducted a laboratory experiment using known activities of ^{222}Rn and ^{220}Rn,

with a controllable ratio of CO_2/air in the carrier gas (Lane-Smith and Sims, 2013).

Based upon our laboratory experiments evaluating the effect of CO_2 on these parameters using the DURRIDGE RAD7 alpha counting system we have determined that when Rn is measured in the presence of CO_2 the ^{220}Rn (thoron) measurement is diminished more than the ^{222}Rn reading and that therefore the $^{220}Rn/^{222}Rn$ decreases as a function of CO_2 concentration (Lane-Smith and Sims, 2013). Our experimental measurements show that for every percentage of CO_2 above zero, the thoron reading should be multiplied by 1.019 (See Figure 5), the radon reading should be multiplied by 1.003 and the measured ratio should be multiplied by 1.016 to correct for the presence of the CO_2. Thus for the measurement of Rn isotopes with significant ambient CO_2 in

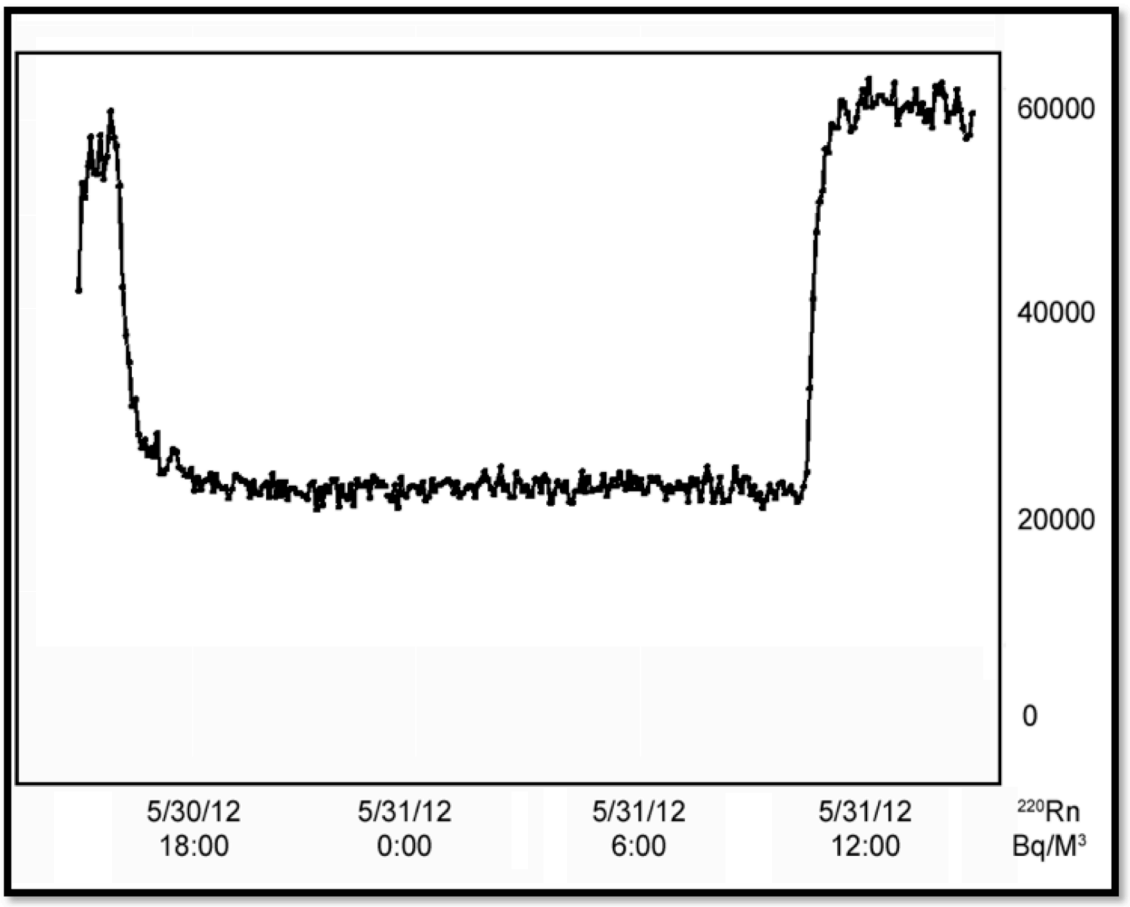

Figure 5. Effect of CO_2 on RAD7 thoron (^{220}Rn) readings. The effect of CO_2 on the thoron reading is dramatic. A change from fresh air to 100% CO_2 reduced the reading from 61,000 Bq/m3 to 21,000 Bq/m3. That's a decrement of 65.6%. In other words a thoron reading at 100% CO_2 should be multiplied by a factor of 2.9 to obtain the fresh-air reading. A correction of 1.9% should be added to a thoron reading in the presence of CO_2 for every percent.

both volcanic and anthropogenic systems, this correction must be applied to obtain optimal accuracy. The result indicates that this correction will modify but not nullify the analysis and conclusions of prior work (e.g. Giammanco et al., 2007). We note that an alternative option is to scrub the CO_2 prior to the measurement of radon as was done in Tuccimei and Soligo (2008). However, the scrubbing of CO_2 prevents simultaneous measurement of CO2 with radon and thoron, whereas the experimental results we present here suggest that a simple correction can be applied. Also, if the CO_2 concentration is high, removing it will reduce the volume of the gas and hence increase the radon concentration in the gas remaining. These measurements have global implications for past (Ciggolini et al., 2009; D'Amore and Sabroux, 1976; Giammanco et al., 2007; 2009; Huxol et al., 2012; Laiolo et al., 2012; Liotta et al., 2010; Martelli et al., 2008; Martinelli 1998; Neri et al., 2011; Perez et al., 2007; Tuccimei and Soligo, 2008; Yang et al., 2011) and future work.

2.3.2 Rn and CO_2 Soil Flux over a Natural CO_2 Reservoir

Radon and CO_2 flux measurements were collected over the LaBarge CO_2 Field, a natural CO_2 reservoir on the Moxa Arch of Southwest Wyoming. Fieldwork was performed summer 2010 and 2011. Here we summarize the key results of that study; details are provided in Quarterly Progress Reports for July-September 2010 and October-December 2011.

Radon and CO_2 flux measurements were collected along three transects, the Muddy Creek Road Transect, the LaBarge Creek Road Transect, and the Kemmerer Transect (see map in Appendix B). The first two transects start above the reservoir and cross the western margin of the reservoir. The Kemmerer Transect was completed away from the CO_2 reservoir. All three transects cross faults to the west and south of the CO_2 reservoir.

Measurements made along the Muddy Creek Road and LaBarge Creek Road Transects suggest that variations in ^{222}Rn, ^{220}Rn, and CO_2 are spatially correlated to the CO_2 reservoir and to structural features proximate to the reservoir. Measurements from the Muddy Creek Road Transect suggest a general trend of increasing CO_2 flux westward coming from a seemingly shallow source with an increasing amount of activity along the faults (Figure 6). The radon signature across most of the LaBarge Creek Road Transect suggests a shallow source of CO_2, but at the west side there is evidence of a deeper source of CO_2 (Figure 7a). The deep signature could indicate that CO_2 is rising up from the LaBarge CO_2 Field. Also, CO_2 flux increases along the faulted region similar to what was seen on Muddy Creek Road Transect additionally suggesting CO_2 seeping up along the faults from the LaBarge CO_2 Field (Figure 7). In comparison to the Muddy Creek Road Transect, the data does not indicate a decrease in CO_2 flux once past the western margin of the LaBarge CO_2 Field, but still shows a similar trend of decreasing in CO_2 flux out of the faults to the east.

The Kemmerer Transect was conducted away from the LaBarge CO_2 Field (see map in Appendix B) to test these apparent correlations. Measurements suggest a decreasing trend eastward in CO_2 flux with some variability along the faults. This area has no deep source of CO_2, but shows flux values (0.1- 0.7 $g/m^2/d$) similar to those measured in the first two transects performed near the LaBarge CO_2 Field. This relationship indicates that the measurements made near the LaBarge CO_2 Field are related to shallow, background levels of CO_2 and not to CO_2 in the field (Figure 8a). Higher values of ^{220}Rn measured on this transect suggest a shallow source of Rn, and the

two isotopes of Rn (^{220}Rn and ^{222}Rn) follow the same characteristic trend (Figure 8b). Upon crossing regions of mapped elevated background gamma radiation (indicated in Figure 8 with the blue and orange field boundaries), Rn measurements do not show any correlations. This relationship also suggests that Rn measurements cannot be correlated to CO_2 flux along this transect. These results suggest that measurements of ^{222}Rn, ^{220}Rn, and CO_2 flux may not be a robust method for monitoring the integrity of geologic carbon sequestration scenarios.

TEXT CONTINUES ON PAGE 19

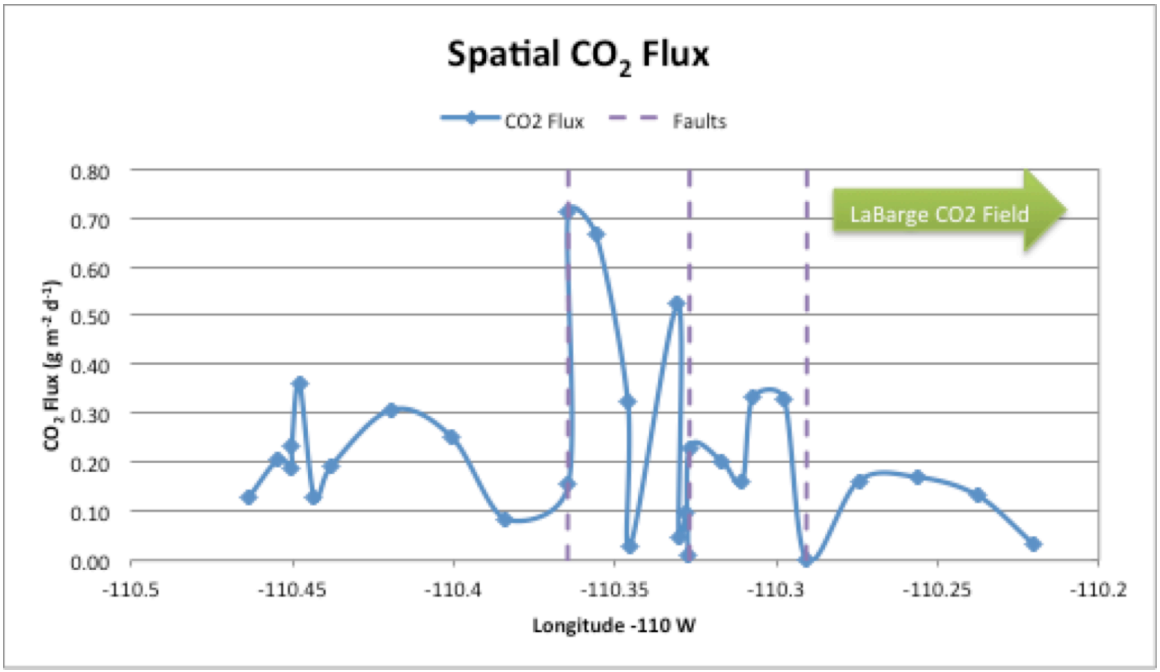

Figure 6. CO_2 flux graphed spatially with respect to longitude. Purple dashed lines represent faults correlated with Appendix B and green arrow represents the start of the water-gas contact of the CO_2 reservoir continuing further eastward

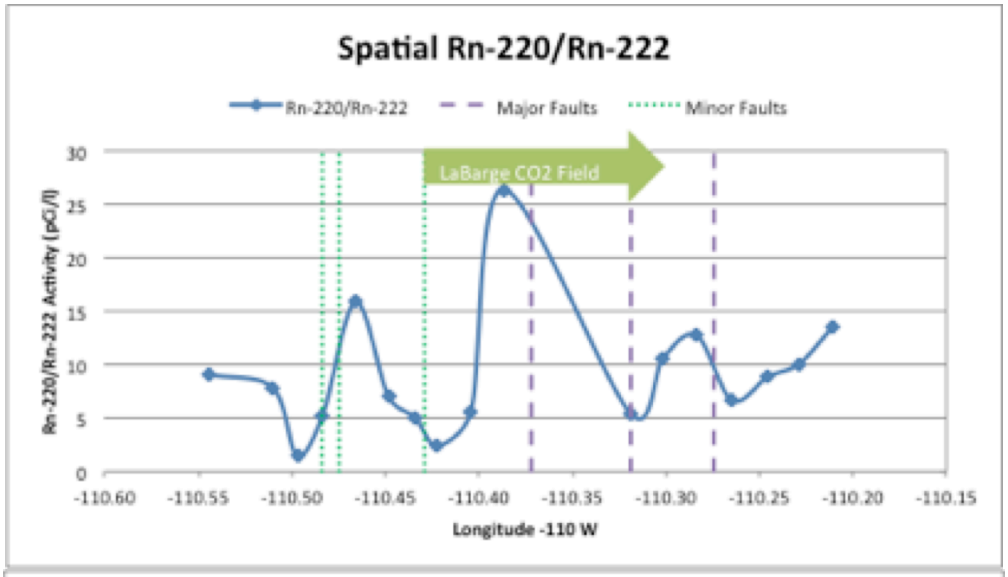

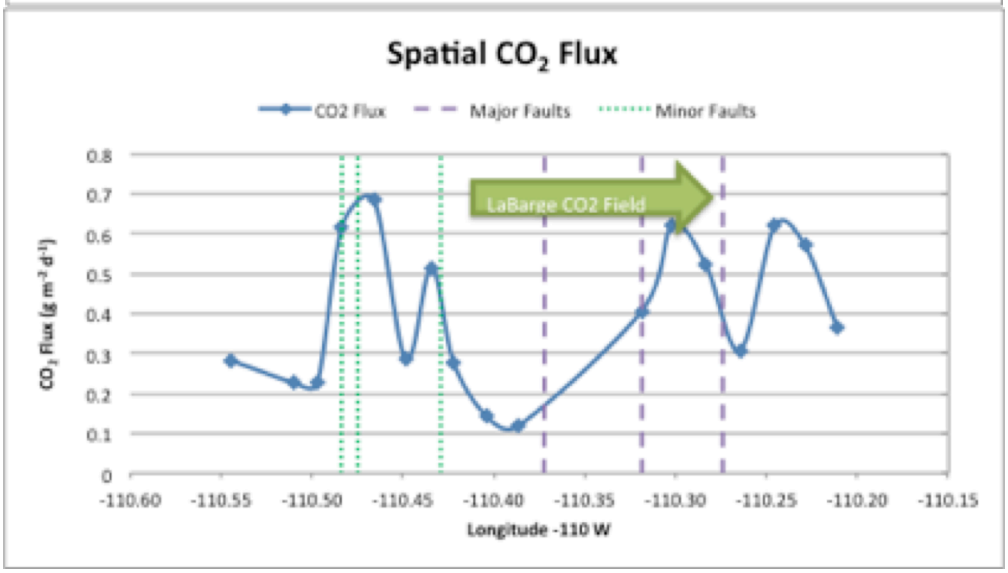

Figure 7. a) Spatially graphed radon ratio (Rn-220/Rn-222) with respect to longitude. Purple dashed lines indicate faults seen on map in Appendix B, green dotted line minor faults seen in the region, and green arrow represents the start of the LaBarge CO_2 field continuing eastward. b) Spatially graphed CO_2 flux along LaBarge Creek Road with respect to Longitude. Symbols are the same as in Figure 6. An increase in flux is seen along or near most of the faults

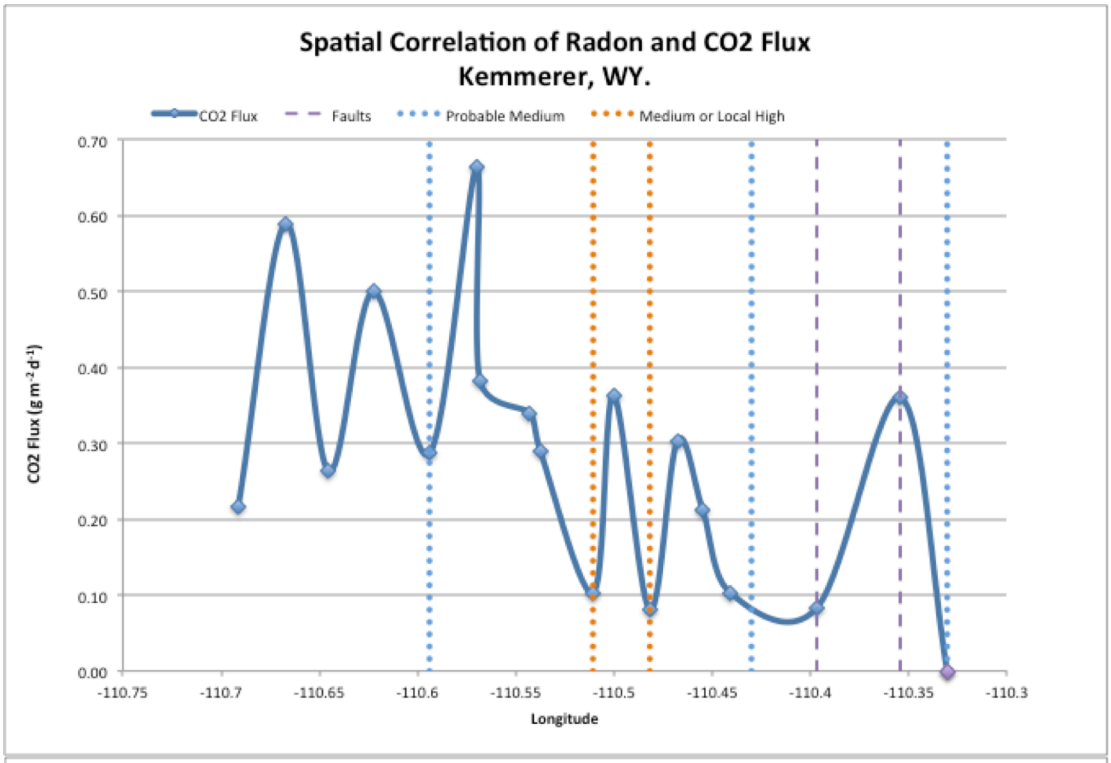

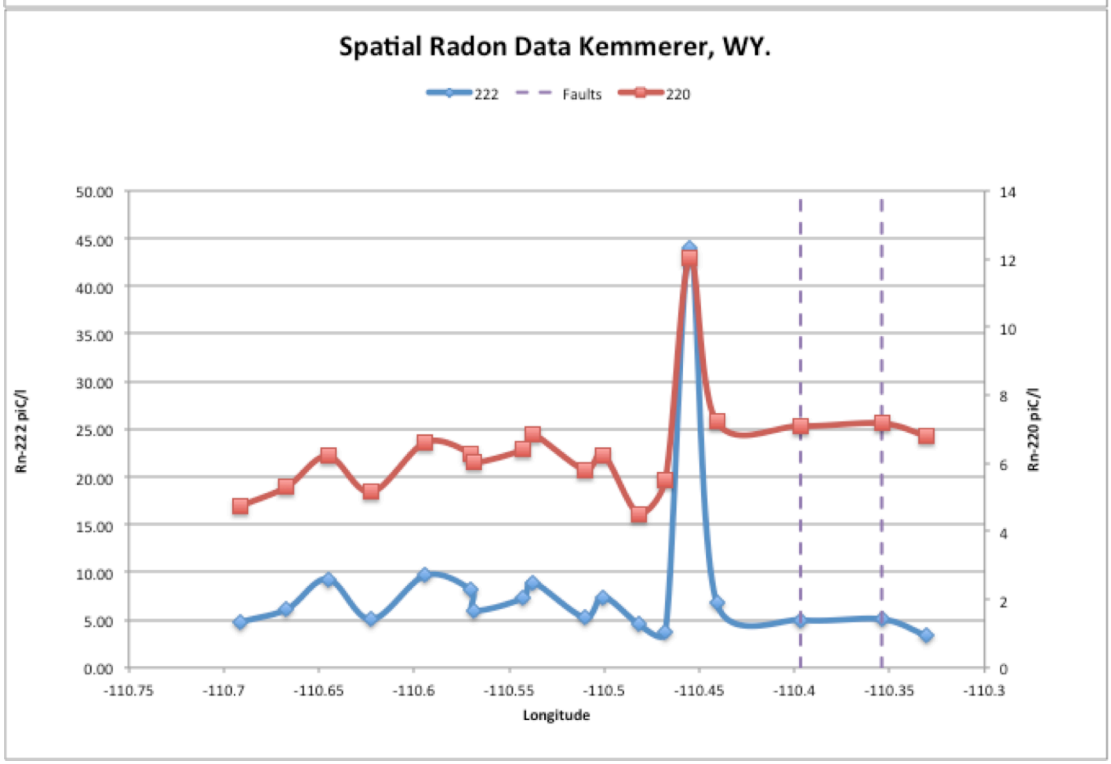

Figure 8a (top). CO_2 flux graphed spatially with respect to longitude. Purple dashed lines represent faults correlated with map in Appendix B, blue dotted lines represent boundaries of mapped probable medium background gamma radiation, and orange dotted lines represent boundaries of mapped medium or local high background gamma radiation (Cannia, J.C., and J.C. Case, 1986). Figure 8b (bottom). Discrete Rn graphed spatially with respect to longitude.

2.3.3 Natural Waters in Areas of Active CO_2-Upwelling

Radon and CO_2 flux measurements were collected from upwelling CO_2-charged springs of the Thermopolis, Wyoming hydrothermal system. Fieldwork was performed thoroughout 2010 and 2011. Here we summarize the key results of this study; details are provided in the Quarterly Progress Reports for April-June 2010, October-December 2010, January-March 2011, and April-June 2011 as well as the MS thesis of Pluda (2012).

Aqueous radon and radium are both present in measureable quantities within the thermal waters of the Thermopolis hydrothermal system; however, the methodology of the isotopes measured in this study needs to be analyzed more systematically to better understand the error that may be associated with these measurements. CO_2 flux measurements exhibited large errors, and measurement of $^{220}Rn/^{222}Rn$ and CO_2 flux did not have any obvious correlation. While no meaningful data regarding radon and CO_2 flux measurements were collected for this part of the project, the utility of this work was to help focus attention on the effect of CO_2 on Rn measurements (Section 2.3.1).

This investigation provided the first geochemical analyses of the thermal waters of the Thermopolis hydrothermal system in over 30 years and evaluated the aqueous geochemistry of this hydrothermal system in an historic and regional geochemical context. Gas bubbles rich in carbon dioxide are continuously rising from the bottom of the Big Spring and all of the thermal waters emit the characteristic odor of hydrogen sulfide gas. No evidence for heating by igneous activity has been identified for the Thermopolis hydrothermal system. However, the source of the abundant carbon dioxide has not been identified and our results do not shed light on its origin. Thermal waters of three active hot springs, Big Spring, White Sulfur Spring, and Teepee Fountain, are similar in composition. The geochemistry of these thermal waters is characteristic of carbonate aquifers or rocks containing abundant carbonate minerals. Previous studies postulate that the thermal waters for the Thermopolis hydrothermal system are a mixture of waters from Paleozoic formations. However, the major element analyses available for waters from these formations are not sufficient to determine whether the thermal waters are a mixture of the Paleozoic aquifers. Further details are provided in the aforementioned Progress Reports and in Pluda (2012) and Kaszuba et al. (2014).

2.3.4 Measurements in Environments with Significant Rn and CO_2

Initial measurements of radon and CO_2 in Yellowstone during the summer of 2010 indicated that there was a weak inverse relationship between ($^{220}Rn/^{222}Rn$) and CO_2 flux emitted from fumaroles and hot springs (see Quarterly Progress Reports for July-September 2010 and October-December 2010. This relationship is consistent with a two-component mixing model as described by Giammanco et al. (2007). However, this model does not presume to describe the behavior of radon and CO_2 dissolved in hydrothermal fluids, and is restricted to diffusive CO_2 efflux from soil degassing and fumaroles (i.e. degassing via permeable pathways: faults and fractures). Because the parents of ^{220}Rn and ^{222}Rn, ^{224}Ra and ^{226}Ra respectively, are both enriched in YS hydrothermal fluids and most hot springs – it follows that in situ production of both of these isotopes could be a significant source dissolved radon.

Additionally, as described above (section 2.3.1 – *Effect of CO_2 on RAD7 Radon Measurements*) the initial radon measurements are probably, in some instances (especially at fumaroles), erroneously low due to the high CO_2 concentrations; the systematic error of artificially low Rn measurements on the RAD7 can now be corrected for, provided the percentage of CO_2[1] in the closed air-loop with the RAD7 is measured simultaneously (Lane-Smith and Sims, 2013). The weak inverse relationship noted previously between ($^{220}Rn/^{222}Rn$) could be, at least partially, an artifact of ^{220}Rn activities that are erroneously lowered by higher CO_2 concentrations. Measurements from sampling in Yellowstone during fall (2013) and summer (2014) did not reveal a relationship between ^{222}Rn and dissolved CO_2 in hot springs (Figure 9). The highest (^{222}Rn) measured was at the Boiling River [2,494 ± 314.1 dpm/L] and the lowest was Narrow Gauge Terrace [5.1 ± 1.0 dpm/L] (Table 2)

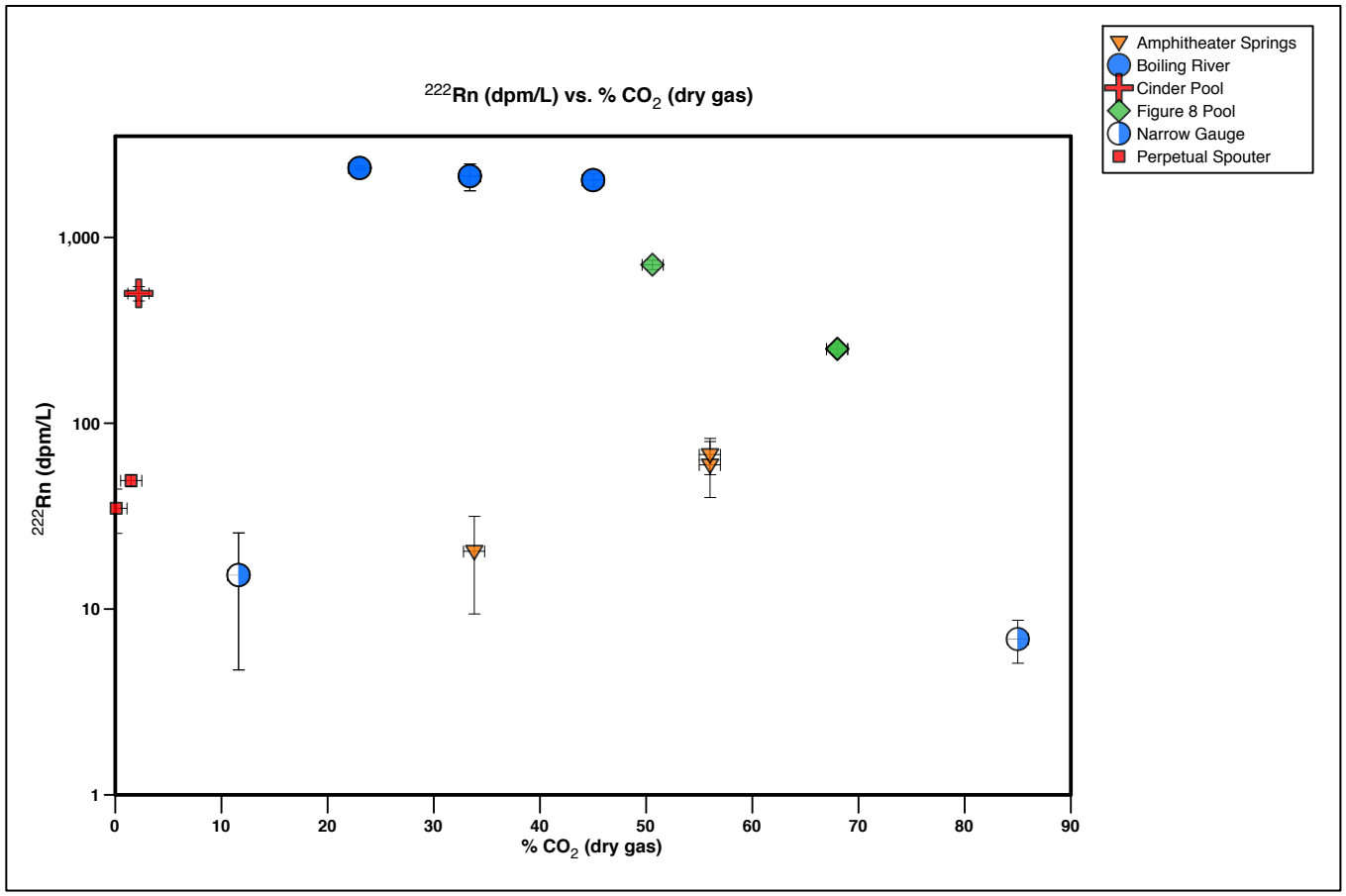

Figure 9. Relationship between 222Rn (dpm / L) activity and % CO_2 (dry gas) from hot springs at Yellowstone National Park. No distinct correlation is apparent.

[1] Percentage CO_2 in this case means the % of CO_2 in dry gas with water vapor removed (to <10% ambient humidity) as well as other gases common in fumaroles and hot springs such as H_2S

Spring Name	Easting (NAD 83)	Northing (NAD 83)	Sample (Date)	^{222}Rn (dpm/L)	2σ Uncert. (dmp/L)	% CO2 (dry gas)
Acid Pool	523025	4952608	BB_YSRn_AP_7.24.14	45.5	8.1	
Acid Pool	523025	4952608	BB_YSRn_AP_9.17.14	40.7	4.4	
Amphitheater Spring	521484	4960698	BB_YSRn_AS_7.25.14_1	59.8	20.0	56
Amphitheater Spring	521484	4960698	BB_YSRn_AS_7.25.14_2	67.8	15.0	56
Amphitheater Spring	521484	4960698	BB_YSRn_AS_8.29.14	20.5	11.1	33.8
Big Bubbler	518589	4949645	BB_YSRn_BB_9.18.14	262.5	13.0	
Boiling River	524491	4981348	BB_YSRn_BR_11.15.13	2361.3	65.9	23
Boiling River	524491	4981348	BB_YSRn_BR_11.17.13_1	1152.8	121.0	26
Boiling River	524491	4981348	BB_YSRn_BR_11.17.13_2	1540.0	184.8	26
Boiling River	524491	4981348	BB_YSRn_BR_8.27.14_1	2092.2	66.0	45
Boiling River	524491	4981348	BB_YSRn_BR_8.27.14_2	1980.0	165.6	45
Boiling River	524491	4981348	BB_YSRn_BR_11.8.14_1	1771.7	350.6	33.4
Boiling River	524491	4981348	BB_YSRn_BR_11.8.14_2	2494.1	314.1	33.4
Beryl Springs	520093	4947288	BB_YSRn_BS_11.18.13	330.0	35.2	
Beryl Springs	520093	4947288	BB_YSRn_BS_11.7.14	349.1	74.9	
Cinder Pool	522976	4953267	BB_YSRn_CP_7.24.14	568.3	128.7	
Echinus Geyser	523590	4952120	BB_YSRn_EG_11.19.13	499.4	44.0	2.2
Echinus Geyser	523590	4952120	BB_YSRn_EG_11.7.14	273.5	40.5	
Figure 8 Pool	544481	4939773	BB_YSRn_F8_7.26.15	251.5	16.9	68
Figure 8 Pool	544481	4939773	BB_YSRn_F8_8.28.14	516.3	6.4	33.8
Figure 8 Pool	544481	4939773	BB_YSRn_F8_9.19.14	712.1	41.3	50.6
Green Dragon Spring	523207	4951896	BB_YSRn_GD_11.7.14	316.1	96.1	
Narrow Gauge	522833	4979596	BB_YSRn_NG_11.16.13	6.9	1.8	85
Narrow Gauge	522833	4979596	BB_YSRn_NG_7.23.14	15.2	10.5	11.6
Narrow Gauge	522833	4979596	BB_YSRn_NG_8.27.14	51.0	17.8	
Narrow Gauge	522833	4979596	BB_YSRn_NG_11.8.14	5.1	1.0	
Obsidian Pool	544528	4939788	BB_YSRn_OP_7.26.14	431.2	90.3	
Obsidian Pool	544528	4939788	BB_YSRn_OP_8.28.14	212.7	18.1	
Obsidian Pool	544528	4939788	BB_YSRn_OP_9.19.14	250.8	18.3	
Perpetual Spouter	523034	4952621	BB_YSRn_PR_7.24.14	49.1	3.7	1.5
Perpetual Spouter	523034	4952621	BB_YSRn_PR_9.17.14	34.8	9.3	0.06
Small Acid Pool	-	-	BB_YSRn_SAP_8.28.14	378.4	11.1	
Sulfur Cauldron	544935	4941831	BB_YSRn_SC_11.18.13	171.6	21.1	
Sulfur Cauldron	544935	4941831	BB_YSRn_SC_11.6.14	236.1	2.9	

Table 2. (^{222}Rn) and % CO_2 measurements from hot springs in Yellowstone National Park

CO_2 (dry gas) ranged from 85% at Narrow Gauge Terrace to 0.06% at Perpetual Spouter (close to ambient air concentrations). At Boiling River, there does not appear to be a positive correlation between % CO_2 and (^{222}Rn) activity (Figure 10). As shown in Figure 11, with the exception of Narrow Gauge, there is a ubiquitous excess of ^{222}Rn relative to parent ^{226}Ra. This indicates that unsupported dissolved ^{222}Rn that is transported from some source, or sources in the hydrothermal system is more significant than shallow aquifer in situ production by ^{226}Ra recoil, either from radium dissolved in solution or radium adsorbed onto aquifer rocks. If CO_2 was acting as a carrier gas for radon, greater radon excesses would be expected for higher concentrations of CO_2 in hot springs waters; this relationship is not evident in Yellowstone hot springs (Figure 12). The anomalous 226Ra excess at Narrow Gauge may be related to the complex morphology of Narrow Gauge.[2]

Additionally, the short half-life of thoron (^{220}Rn: $t_{1/2}$ = 55.6 seconds), makes accurate measurement particularly problematic. Successful thoron measurement requires a short path-length from the source (i.e. hot spring, fumarole, soil) and / or a fast water and airflow rate such

[2] Narrow Gauge Terrace includes many discharge zones, some of which exhibit vigorous degassing and others that do not. Sampling is restricted to one of the only safe and accessible areas. Because the lowest radon activities are observed at Narrow Gauge it is likely that both radon and CO_2 are exsolving from the water escaping through gas vents or another outlet that is inaccessible.

that thoron can reach the RAD7 detector before decaying to activities below detection. However, airflow rates > 3 LPM are not compatible with RAD7 detection and at fumaroles even rates between 1-3 LPM can be incompatible with RAD7 measurement because large amounts of water vapor in fumarole gases cannot be dehumidified adequately (≤ 10 % humidity) at such such rates. In recognition of these limitations, our future measurements will include methodological refinements designed to optimize the parameters necessary for successful thoron measurement.

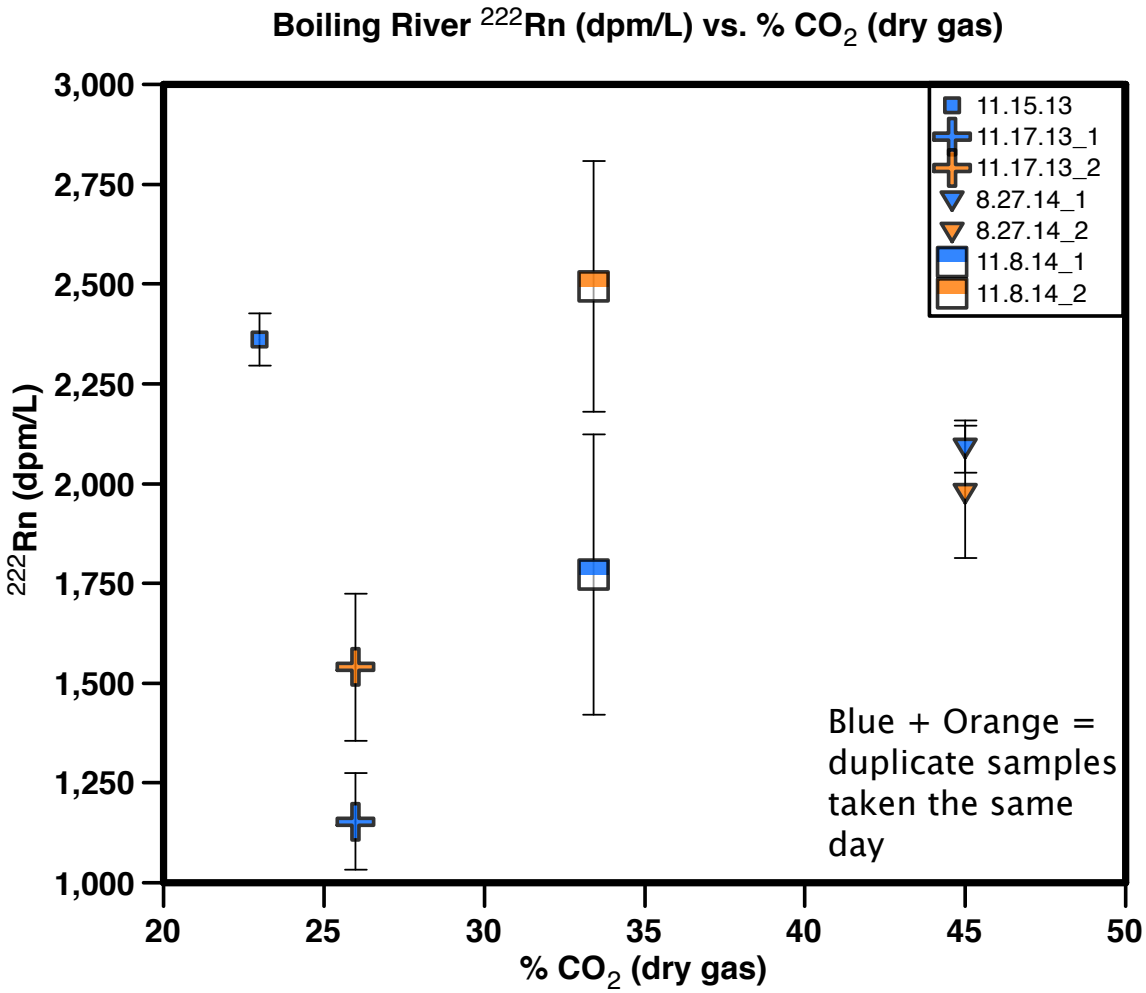

Figure 10. (^{222}Rn) activity versus % CO_2 (dry gas). No positive correlation is evident.

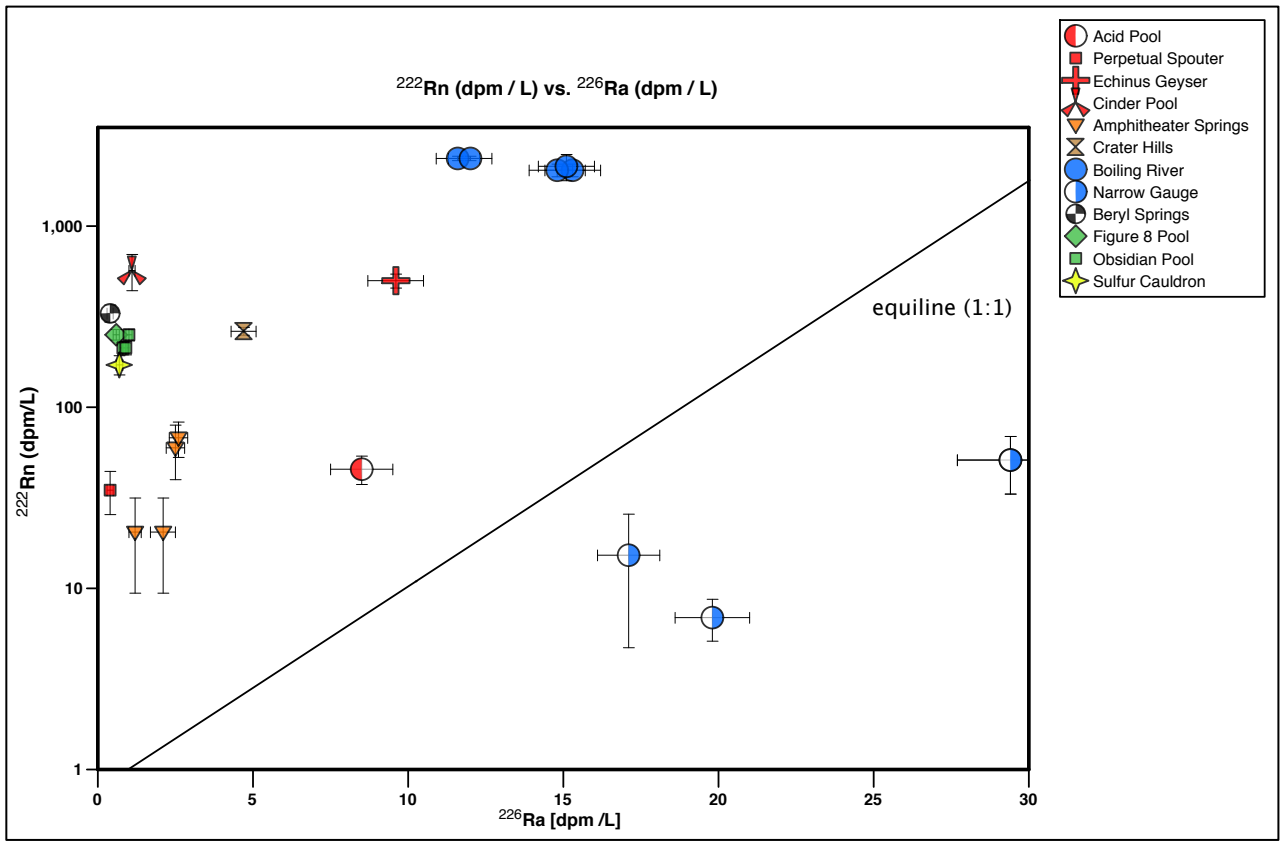

Figure 11. (^{222}Rn) vs. (^{226}Ra) for Yellowstone hot springs – showing substantial ^{222}Rn excesses (points plotting above the equiline) for all hot springs except Narrow Gauge.

TEXT CONTINUES ON PAGE 24

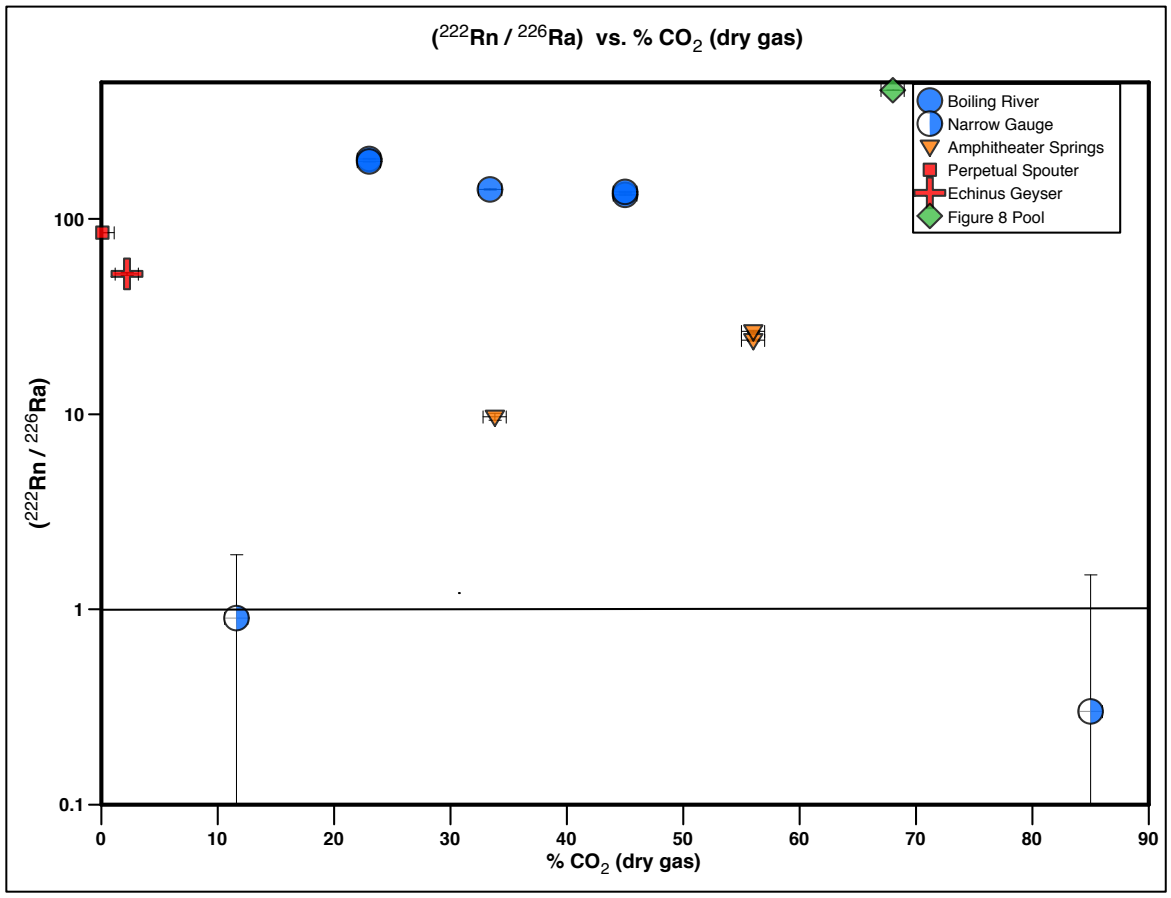

Figure 12. (^{222}Rn / ^{226}Ra) vs. % CO_2 (dry gas) for select Yellowstone hot springs. Excess ^{222}Rn relative to ^{226}Ra parent does not show an obvious correlation with hot spring CO_2 concentration.

2.3.5 Laboratory Insights for Rn and CO_2

Surface area, surface:volume ratios, and lithology. Surface area and surface:volume ratios of source geomaterials, and thus the size of individual grains of these materials, influence the ability of Rn to escape the crystal lattice. These factors are a major influence on the nature and relevance of the temporal constraints developed by ^{222}Rn and ^{220}Rn activity measurements. As described in Section 2.2.4, 4-6 mm, 0.85-1 mm, and 45-75 µm size fractions of Banco Bonito Obsidian Cerros Del Rio Basalt, and Guaje Pumice were evaluated. The data were originally presented and discussed in the Quarterly Progress Report for October-December, 2013. However, given the importance of the data to the following summary, we again provide the dataset in this report (see Table 1 and Figures 1, 2, and 3, all in Appendix C).

Data for the the different rock types (Banco Bonito Obsidian, Cerros Del Rio Basalt and Guaje Pumice, Jemez Volcanic Field, NM, USA) show that the finest grain size is correlated with ^{222}Rn and ^{220}Rn emissivity (Figures 1, 2, and 3 in Appendix C). In all experiments the finest grain size always has the highest emissivity; however, the two coarser grain sizes have similar emissivity. The behavior of the emissivity did not change between the two experiments. This observation suggests that a systematic relationship exists, but grain size alone is likely not representative of

specific surface area enough to establish a solid relationship. We note that this based on a small number of measurements and that this is a continuing effort. We will continue to replicate these measurements and also look at measures of surface area to more effectively evaluate the samples surface area/volume ratio.

Reaction of source rock with formation waters and CO_2. CO_2-H_2O-rock reactions may also influence Rn activity by such processes as changing surface area (thus surface:volume ratios) and armoring reactive surfaces. As described in Section 2.2.4, one size fraction of Cerros Del Rio Basalt (45-75μm) was reacted with water (designated as H_2O+Rock experiments) and with CO_2-saturated water (designated as CO_2+H_2O+Rock experiments) in separate experiments. The results of these experiments are tabulated in Appendix D. The data are plotted and critical aspects discussed in the remainder of this section. This dataset is presented for the first time in this Final Report.

Emissivity for both ^{222}Rn and ^{220}Rn increases with temperature in the H_2O+Rock experiments. H_2O+Rock experiments at low (10 mmol/kg NaCl, Figure 13) and higher (28 mmol/kg NaCl, Figure 14) salinity exhibit a linear increase from 25 to 60°C. This relationship is expected and may be explained by one of two mechanisms, or some combination thereof; we cannot assess the relative importance of these two mechanisms with the dataset generated by these experiments. First, Radon diffusion out of the rock may be a temperature–dependent process. Temperature controls diffusion according to Fick's First Law in many geological systems. Second, water-rock reaction yields greater amounts of dissolution of the rock with increasing temperature, and this dissolution releases proportionally more Radon into the water. Applying the general rule of thumb that every 10°C increase in temperature approximately doubles kinetic rates, reactions leading to rock dissolution are roughly one order of magnitude faster at 60°C relative to 25°C. Dissolution of minerals and rocks is often accompanied by formation of new minerals that can grow over reactive surfaces and inhibit further dissolution. We did not observe mineral growth in these experiments; if secondary minerals precipitated, they did not appear to interfere with dissolution and release of Radon.

In comparison, emissivity for both ^{222}Rn and ^{220}Rn in the CO_2+H_2O+Rock experiments are approximately the same at 25 and 40°C; emissivity for both isotopes increases between 40 and 60°C (Figure 15). Emission is greater at all temperatures for the CO_2+H_2O+Rock experiments compared to the H_2O+Rock experiments (compare Figures 14 and 15). The presence of CO_2 changes the relative importance of the controlling factors of Radon release. Emission does not increase between 25 and 40°C despite the importance of temperature to diffusion and mineral dissolution. CO_2-rich waters can form carbonate minerals that can overgrow reactive surfaces and prevent further dissolution as well as "armor" surfaces against diffusion. However, secondary carbonate growth was not observed in these experiments. Carbonate minerals are actually more stable and more likely to crystallize at higher temperatures. However, greater Radon emission took place at 60°C relative to 25 and 40°C. Also, given that emission is higher at all temperatures in the CO_2+H_2O+Rock experiments compared to the H_2O+Rock experiments, rock dissolution is likely increased. To conclude, simple relationships appear to govern the emission of Radon due to water-rock reaction, but CO_2 adds complexities that perturb water-rock reactions, at least at lower temperatures.

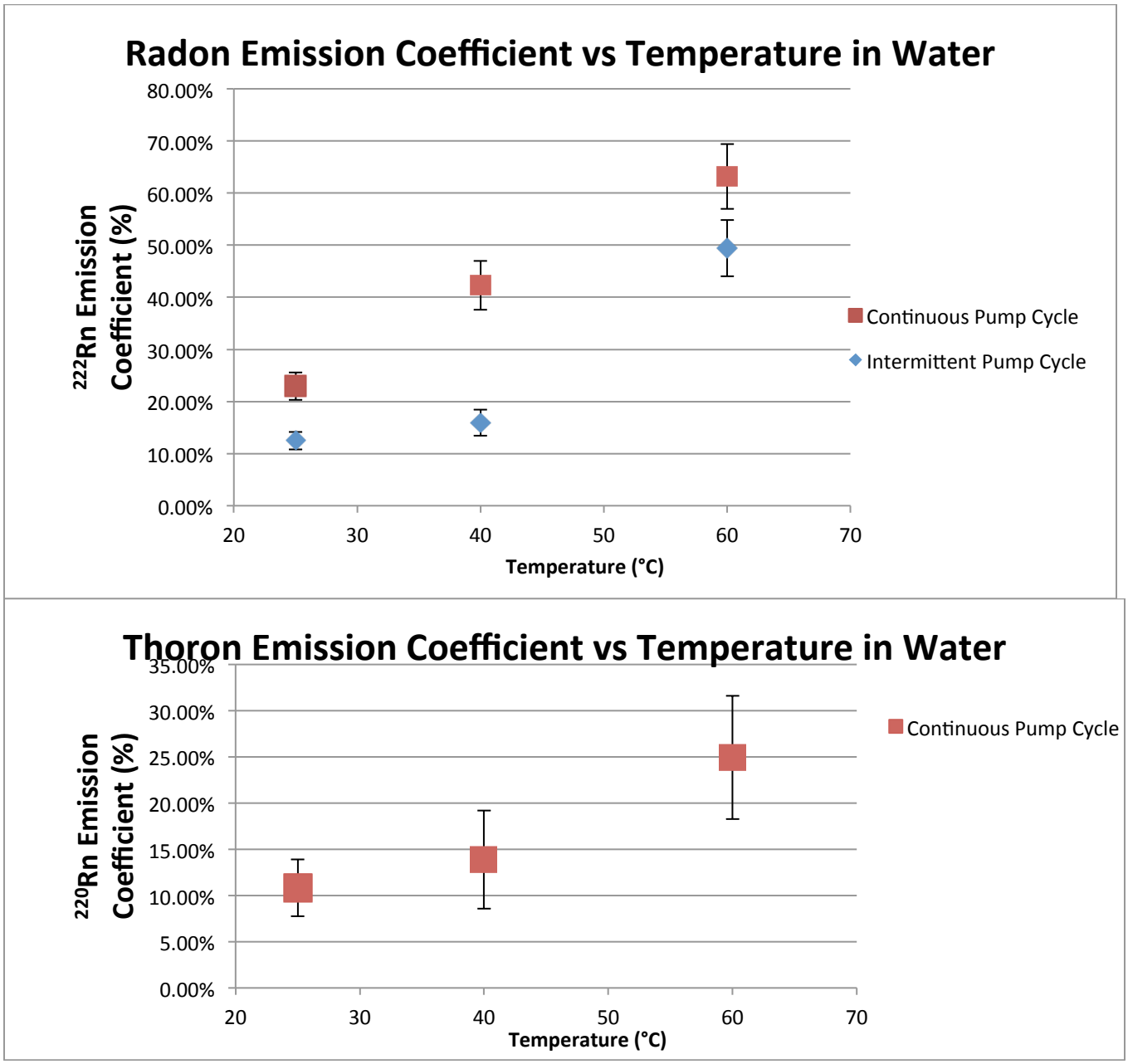

Figure 13: Radon emissivity versus water temperature for low salinity (10 mmol/kg NaCl) H_2O+Rock experiments. Continuous pump cycle points are the measurements made when the pump was on continuously during the run. Intermittent pump cycle points are the measurements made when the pump was on for 4 minutes every 20 minutes during the run.

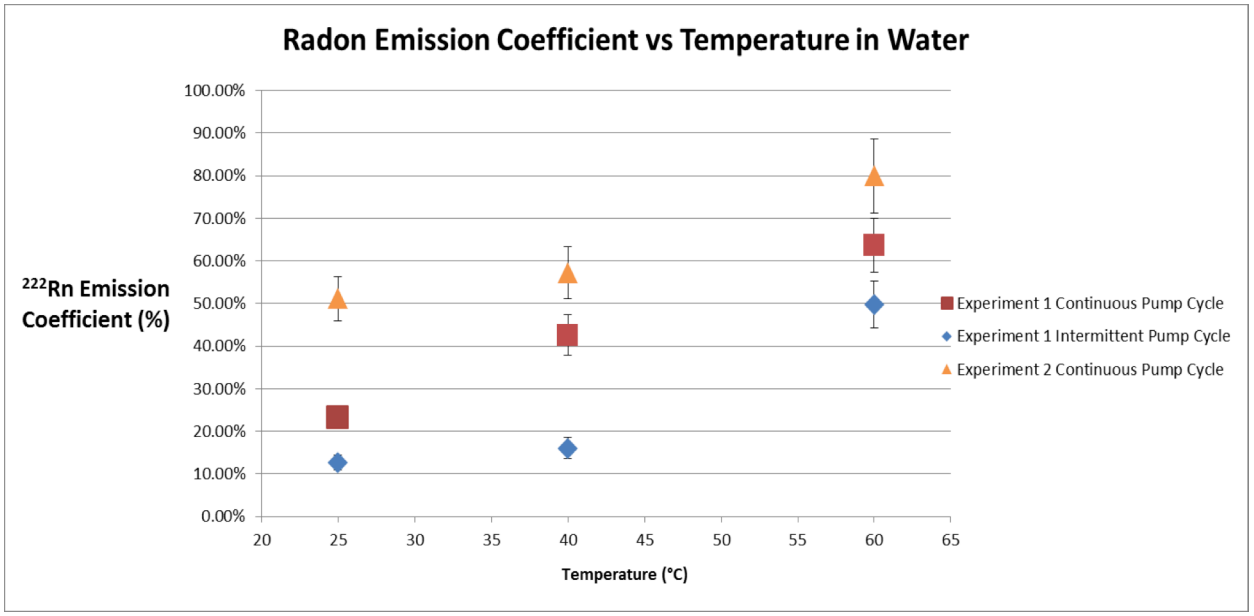

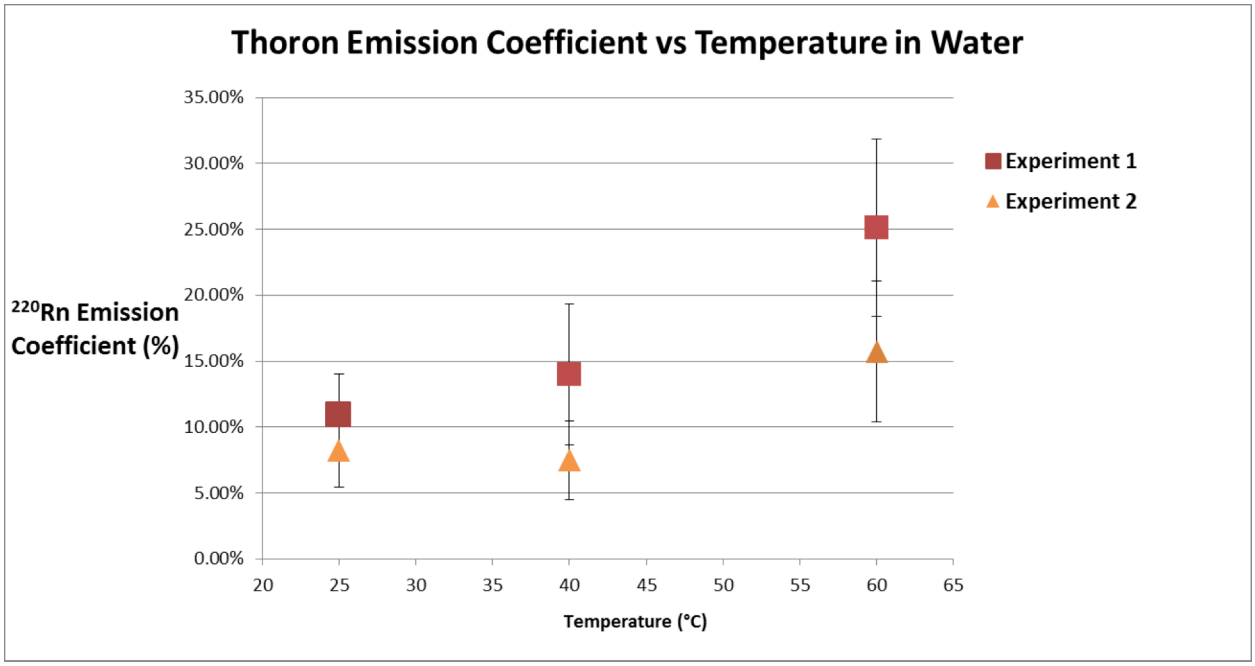

Figure 14. Radon emissivity versus temperature for 28 mmol/kg NaCl H_2O+Rock experiments.

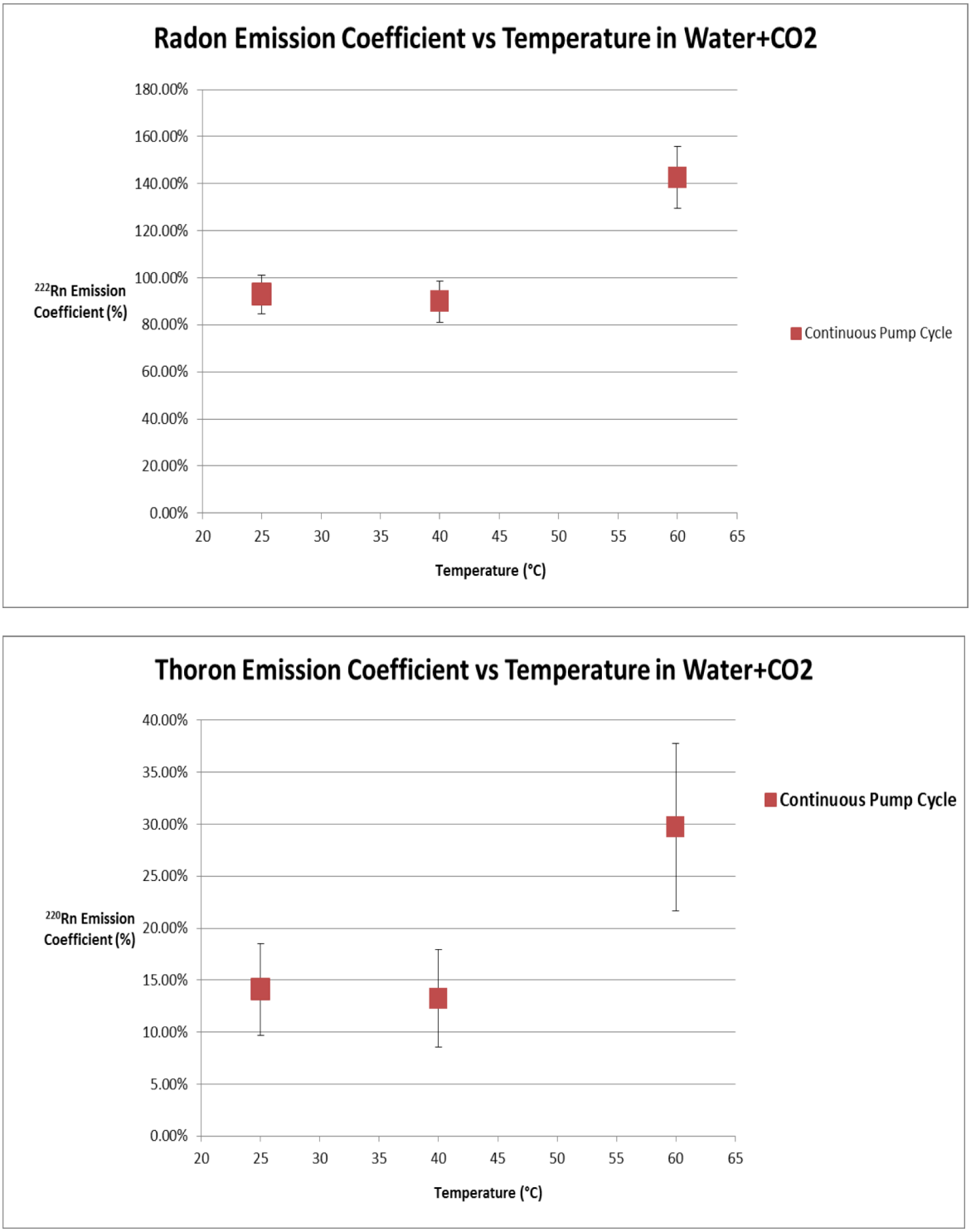

Figure 15. Radon emissivity versus temperature for 28 mmol/kg Na_2CO_3 CO_2+H_2O+Rock experiments

2.3.6 Graduate and Undergraduate Student Training

This project provided training opportunities for four graduate and four undergraduate students. Training was accomplished by these students doing the actual fieldwork and laboratory work for the project. Although the scientific work differed in detail, all were mentored in fundamental geologic and geochemical skills that will be required for implementing and deploying CCS technologies. Table 3 lists each of the eight students and summarizes their involvement in the project as well as their accomplishments. Two of the four graduate students (Maloney and Pluda) completed Master of Science degrees focused on the project. Both are full-time professionals with a geologic consulting company; they are poised to do work in a CCS technology area. One of the four graduate students (Scott) is currently working on his PhD at the University of Wyoming and one (Mandl) left the program.

Table 3. Graduate and undergraduate students on the project (in alphabetical order).

Name	Role in Project	Degree Earned[1]	Current Status	Comments
Matthew Carberry	Initial work on laboratory tests	BS	Unknown	Minimal work on project
Tim Moloney	Early fieldwork in Yellowstone	MS	Permanent position w/ Trihydro Corporation (geologic consulting)	MS thesis focused on this project (Moloney 2011)
Max Mandl	Continued work on laboratory tests	---	PhD student, ETH Zurich	Left program
Virginia Marcon	Fieldwork in SW Wyoming (Moxa Arch) and Thermopolis, WY	BS	Post-MS at UW	Will enter PhD program (not UW) Fall 2015
Allison Pluda	Fieldwork in SW Wyoming (Moxa Arch) and Thermopolis, WY	MS	Permanent position w/ Trihydro Corporation (geologic consulting)	MS thesis focused on this project (Pluda 2012), data that was produced lead to journal article (Kaszuba et al., 2014)
Michael Schedel	Assisted with laboratory tests	BS	Unknown	Minimal work on project
Sean Scott	Fieldwork in Yellowstone	---	PhD in progress at UW	---
Evan Soderberg	Completed majority of work on laboratory tests.	BS	Working as tech in the Dept.	Instrumental in success of lab tests. Applying to graduate programs

[1]Department of Geology and Geophysics

The research experience provided by this project to one of the four undergraduate students (Marcon) contributed to her decision to complete an MS at the University of Wyoming. Her MS focused on a different research area. At the time of this report she has been accepted into four prominent PhD programs (Ohio State University, Penn State University, Rice University, and Virginia Tech). A second undergraduate student (Soderberg) was instrumental in the success of the laboratory program. He developed much of the experimental design, collected the data, and developed the interpretations. He also presented the results of his work at the 2013 and 2014 NETL Project Review Meetings. He is currently working as a technician in the Department of Geology and Geophysics and is applying to MS programs across the US. The other two undergraduate students (Carberry and Schedel) did not accomplish much on the project; both have since graduated from the University of Wyoming. We do not know their current employment status.

3. CONCLUSIONS

This integrated field-laboratory program evaluated the use of radon and CO_2 flux measurements to constrain source and timescale of CO_2 fluxes in environments proximate to CO_2 storage reservoirs. By understanding the type and depth of the gas source, the integrity of a CO_2 storage reservoir can be assessed and monitored. The concept is based on correlations of radon and CO_2 fluxes observed in volcanic systems. This fundamental research is designed to advance the science of Monitoring, Verification, and Accounting (MVA) and to address the Carbon Storage Program goal of developing and validating technologies to ensure 99 percent storage performance. Graduate and undergraduate students conducted the research under the guidance of the Principal Investigators; in doing so they were provided with training opportunities in skills required for implementing and deploying CCS technologies.

Although a final method or "tool" was not developed, significant progress was made. The field program identified issues with measuring radon in environments rich in CO_2. Laboratory experiments determined that when Rn is measured in the presence of CO_2 the ^{220}Rn measurement is diminished more than the ^{222}Rn reading and that therefore the $^{220}Rn/^{222}Rn$ decreases as a function of CO_2 concentration (Layne Smith and Sims, 2013). Thus a correction factor was developed for use in field and laboratory environments where radon and CO_2 measurements are made. Specifically, for every percentage of CO_2 above zero, the ^{220}Rn reading should be multiplied by 1.019, the ^{222}Rn reading should be multiplied by 1.003, and the measured ratio should be multiplied by 1.016 to correct for the presence of the CO_2.

The field program identified issues with radon and CO_2-flux measurements in soil gases at a natural CO_2 analog. A systematic survey of radon and CO_2 flux in soil gases at the LaBarge CO_2 Field in Southwest Wyoming indicates that Rn measurements could not be correlated to CO_2 flux. Our results indicate that measurements of ^{222}Rn, ^{220}Rn, and CO_2 flux may not be a robust method for monitoring the integrity of a CO_2 storage reservoir.

The field program was not able to correlate radon and CO_2 flux in the CO_2-charged springs of the Thermopolis hydrothermal system. However, this part of the program helped to motivate the laboratory experiments that determined correction factors for measuring radon in CO_2-rich environments. This part of the program also trained and enabled one graduate student (Allison Pluda) to complete a Master of Science degree. Her work produced the first geochemical

analyses of the CO_2-charged springs of Thermopolis in over 30 years. In addition, this part of the field program evaluated the aqueous geochemistry of this hydrothermal system in an historic and regional geochemical context. The geochemistry of the CO_2-charged waters is characteristic of carbonate aquifers or rocks containing abundant carbonate minerals. Previous studies postulate that the CO_2-charged waters for the Thermopolis hydrothermal system are a mixture of waters from Paleozoic formations. However, major element analyses for waters from these formations are not sufficient to determine whether the thermal waters are a mixture of the Paleozoic aquifers. Ms. Pluda is now a full-time professional with a geologic consulting company. With her education on this project and current employment she is poised to begin work in a CCS technology area whenever the opportunity becomes available.

Measurement of radon and thoron in springs has improved significantly since the field program first began; however, in situ measurement of radon, and particularly thoron (^{220}Rn) in springs is problematic. Even duplicate measurements taken in the same location only about 1.5 hours apart are not within error (while the CO_2, meanwhile, remained more or less constant). The possible cause(s) of these variations is not readily apparent. Temporal variations in radon flux and dissolved radon concentrations, even on the timescale of minutes to hours, may be a significant source of radon variation. Additionally, our measurements of spring chemistry indicate that at most springs the water chemistry (pH, ORP, resistivity, conductivity, and major cations and anions) varies on the timescale of days to weeks - especially after major precipitation events. Despite the fact that radon is non-reactive, changes in water chemistry may still influence radon exsolution. For example, it has been demonstrated that salinity can have a significant effect on the radon partition coefficient (Schubert et al., 2012) – and therefore the calculation of dissolved radon concentrations may be biased if differences and variations in salinity are not taken into account. Future refinements include simultaneous salinity measurements and systematic corrections, or adjustments to the partition coefficient as needed for more accurate radon concentration determination. Nonetheless, this part of the program also trained and enabled one graduate student (Tim Moloney) to complete a Master of Science degree. With his education on this project and current employment he is poised to begin work in a CCS technology area whenever the opportunity becomes available.

Laboratory experiments evaluated important process-level fundamentals that effect measurements of radon and CO_2. Fine-grained source minerals yield higher radon emissivity compared to coarser-sized source minerals. However, subtleties in the dataset suggest that grain size alone is not fully representative of all the processes controlling the ability of radon to escape its mineral host. In experiments that evaluated reaction of rocks with water, emissivity for both ^{222}Rn and ^{220}Rn increases linearly with temperature. This is consistent with temperature-dependent diffusion from within the minerals and with enhanced mineral dissolution at higher temperatures; dissolution releases proportionally more radon into the water. In comparison, the presence of CO_2 changes the relative importance of the factors that control release of radon. Emissivity for both ^{222}Rn and ^{220}Rn in the CO_2-bearing experiments is greater at all temperatures compared to the experiments without CO_2, but emissivity does not increase as a simple function of temperature. Governing processes may include a balance between enhanced dissolution and carbonate mineral formation in CO_2-rich waters, but the results are not definitive.

GRAPHICAL MATERIALS LIST

REFERENCES

Allis, R., Chidsey, T., Gwynn, W., Morgan, C., White, S., Adams, M., and Moore, J., 2001, Natural CO_2 reservoirs on the Colorado Plateau and Southern Rocky Mountains: Candidates for CO_2 sequestration, Proceedings of the First National Conference on Carbon Sequestration: Washington, D.C., National Energy Technology Laboratory, US Department of Energy.

Blackstone, D. J., 1978. Tectonic Map of the Overthrust Belt Western Wyoming, Southeasern Idaho and Northeastern Utah; Showing current oil and gas drilling and development. Laramie, WY: Geological Survey of Wyoming.

Bourdon, B., Bureau, S., Andersen, M.B., Pili, E., and Hubert, A., 2009, Weathering rates from top to bottom in a carbonate environment: Chemical Geology, v. 258, p. 275-287.

Bureau of Land Management, 2009, Fontenelle Reservoir Surface Managemtnet Status 1:100,000 - Scale Topographic Map. Denver, CO., U.S. Geological Survey and U.S. Department of the Intererior Bureau of Land Managemtn.

Cannia, J.C., and J.C. Case, 1986, Planning Guide map for radon studies in Wyoming. *OFR 86-17* . Wyoming State Geological Survey.

Cigolini, C., P. Poggi, M. Ripepe, M. Laiolo, C. Ciamberlini, D. Delle Donne, G. Ulivieri, D. Coppola, G. Lacanna, E. Marchetti, D. Piscopo, and R. Genco, 2009, Radon surveys and real-time monitoring at Stromboli volcano: Influence of soil temperature, atmospheric pressure and tidal forces on 222Rn degassing, *J. Volcanol. Geoth. Res*. **184**, 3-4, 381-388, DOI:10.1016/j.jvolgeores.2009.04.019.

D'Amore, F., and J.C. Sabroux, 1976, Signification de la présence de radon 222 dans le fluides géothermiques, *B. Volcanol*. **40**, 2, 106-115, DOI:10.1007/BF02599855 (in French).

De Bruin, R. C., 2004, *Carbon dioxide map of Wyoming.* Wyoming State Geological Survey.

De Bruin, R., 1991, *Wyoming's carbon dioxide resources.* Wyoming State Geological Survey.

Dickinson, W. R., 2006, Geotectonic evolution of the Great Basin. *geosphere* , 353-368.

Dosseto, A., Turner, S.P., and Chappell, J., 2008, The evolution of weathering profiles through time: New insights from uranium-series isotopes: Earth and Planetary Science Letters, v. 274, p. 359-371

Environmental Protection Agency, 2010, *Radon (Rn)*. Retrieved Sept 30, 2010, from EPA United States Environmental Protection Agency: http://www.epa.gov/radon/index.html

Giammanco, S., K.W.W Sims, and M. Neri., 2007, *Geochemistry Geophysics Geosystems , 8* (10). Q10001, DOI: 10.1029/2007GC001644

Giammanco, S., G. Immè, G. Mangano, D. Morelli, and M. Neri (2009), Comparison between different methodologies for detecting radon in soil along an active fault: The case of the Pernicana fault system, Mt. Etna (Italy), *Appl. Radiat. Isotopes* **67**, 1, 178-185, DOI: 10.1016/j.apradiso.2008.09.007

Huxol, S., M.S. Brenwald, E. Hoehn, and R. Kipfer, 2012, On the fate of 220Rn in soil material in dependence of water content: Implications from field and laboratory experiments, *Chem. Geol.* **298-299**, 116-122, DOI: 10.1016/ j.chemgeo.2012.01.002.

Ingalls, B. and L. Park, 2010, Biotic and taphonomic response to lake-level fluctuations in the Great Green River Basin (Eocene), Wyoming. *Palaios* , 287-298.

Kaszuba, John P., Sims, Kenneth W. W., and Pluda, Allison, 2014, Aqueous geochemistry of the Thermopolis hydrothermal system, southern Bighorn Basin, Wyoming: Rocky Mountain

Geology, v. 49, p. 1-16.
Laiolo, M., C. Cigolini, D. Coppola, and D. Piscopo, 2012, Developments in real- time radon monitoring at Stromboli volcano, *J. Environ. Radioactiv.* **105**, 21-29, DOI: 10.1016/j.jenvrad.2011.10.006.
Lane-Smith, D., & Sims, K. W. W., 2013. The effect of CO_2 on the measurement of ^{220}Rn and ^{222}Rn, with instruments utilizing electrostatic precipitation. *Acta Geophysica*. V. 61, p. 822-830, available at http://agp.igf.edu.pl/
Liotta, M., A. Paonita, A. Caracausi, M. Martelli, A. Rizzo, and R. Favara, 2010, Hydrothermal processes governing the geochemistry of the crater fumaroles at Mount Etna volcano (Italy), *Chem. Geol.* **278**, 1-2, 92-104, DOI:10.1016/j.chemgeo.2010.09.004.
Love, J.D and A. Christiansen, 1964, Geologic Map of Wyoming. U.S. Geological Survey.
Martelli, M., A. Caracausi, A. Paonita, and A. Rizzo, 2008, Geochemical variations of air-free crater fumaroles at Mt. Etna: New inferences for forecasting shallow volcanic activity, *Geophys. Res. Lett.* **35**, 21, L21302, DOI:10.1029/2008GL035118.
Martinelli, G., 1998, Gas geochemistry and 222Rn migration process, *Radiat. Prot. Dosim.* **78**, 1, 77-82, DOI: 10.1093/oxfordjournals.rpd.a032338.
Moloney, Timothy P., 2011, Uranium and thorium decay series isotopic constraints on the source and residence time of solutes in the Yellowstone hydrothermal system. M.S. Thesis, Department of Geology and Geophysics, University of Wyoming, April 2012.
Neri, M., S. Giammanco, E. Ferrera, G. Patanè, and V. Zanon, 2011, Spatial distri- bution of soil radon as a tool to recognize active faulting on an active vol- cano: the example of Mt. Etna (Italy), *J. Environ. Radioactiv.* **102**, 9, 863-870, DOI: 10.1016/j.jenvrad.2011.05.002.
Pérez, N.M., P.A. Hernández, E. Padrón, G. Melián, R. Marrero, G. Padilla, J. Bar- rancos, and D. Nolasco, 2007, Precursory subsurface 222Rn and 220Rn de- gassing signatures of the 2004 seismic crisis at Tenerife, Canary Islands, *Pure Appl. Geophys.* **164**, 12, 2431-2448, DOI: 10.1007/s00024-007-0280-x.
Pluda, Allison, R., 2012, Aqueous Geochemistry of the Thermopolis Hydrothermal System, Wyoming, M.S. Thesis, Department of Geology and Geophysics, University of Wyoming April 2012.
PP Systems. 2007, Operator's Manual. Amesbury, MA: PP Systems.
Tonani, F. and G. Miele, 1991, *Methods for measuring flow of carbon dioxide through soils in the volcanic setting.* Ann, Ist. Firenze: Glob
Tuccimei, P., and M. Soligo, 2008, Correcting for CO2 interference in soil radon flux measurements, *Radiat. Meas.* **43**, 1, 102-105, DOI: 10.1016/j.radmeas.2007.05.056.Werner, C., Brantley, S. L. & Boomer, K., 2000, CO_2 emissions related to the Yellowstone volcanic system: 2. Statistical sampling, total degassing, and transport mechanisms. *Journal of Geophysical Research* **105,** 10831.
Werner, C. & Brantley, S., 2003, CO_2 emissions from the Yellowstone volcanic system: Yellowstone CO_2 Emissions. *Geochemistry, Geophysics, Geosystems* **4**.
Yang, T.F., H.Y. Wen, C.C. Fu, H.F. Lee, and T.F. Lan, 2011, Soil radon flux and concentrations in hydrothermal area of the Tatun Volcano Group, Northern Taiwan, *Geochem. J.* **45**, 6, 483-490.

APPENDIX A - LABORATORY METHODS FOR REACTION OF SOURCE ROCK WITH FORMATION WATERS AND CO_2

REPRODUCED FROM QUARTERLY PROGRESS REPORT FOR JANUARY-MARCH, 2014

Figure 2

Sample in Water Experiment for ^{222}Rn

Measuring:
One Grain Size (45-75 µm)
Three temperatures (21°C , 50° C and 90° C)
^{222}Rn $t_{1/2}$=3.8235 d

Measure by build-up of Rn at temperature to secular equilibrium in container head space then with a continuous flow, homogenizing air in whole system, equilibrating air and water, and allowing Rad 7 to measure the activity in the air.

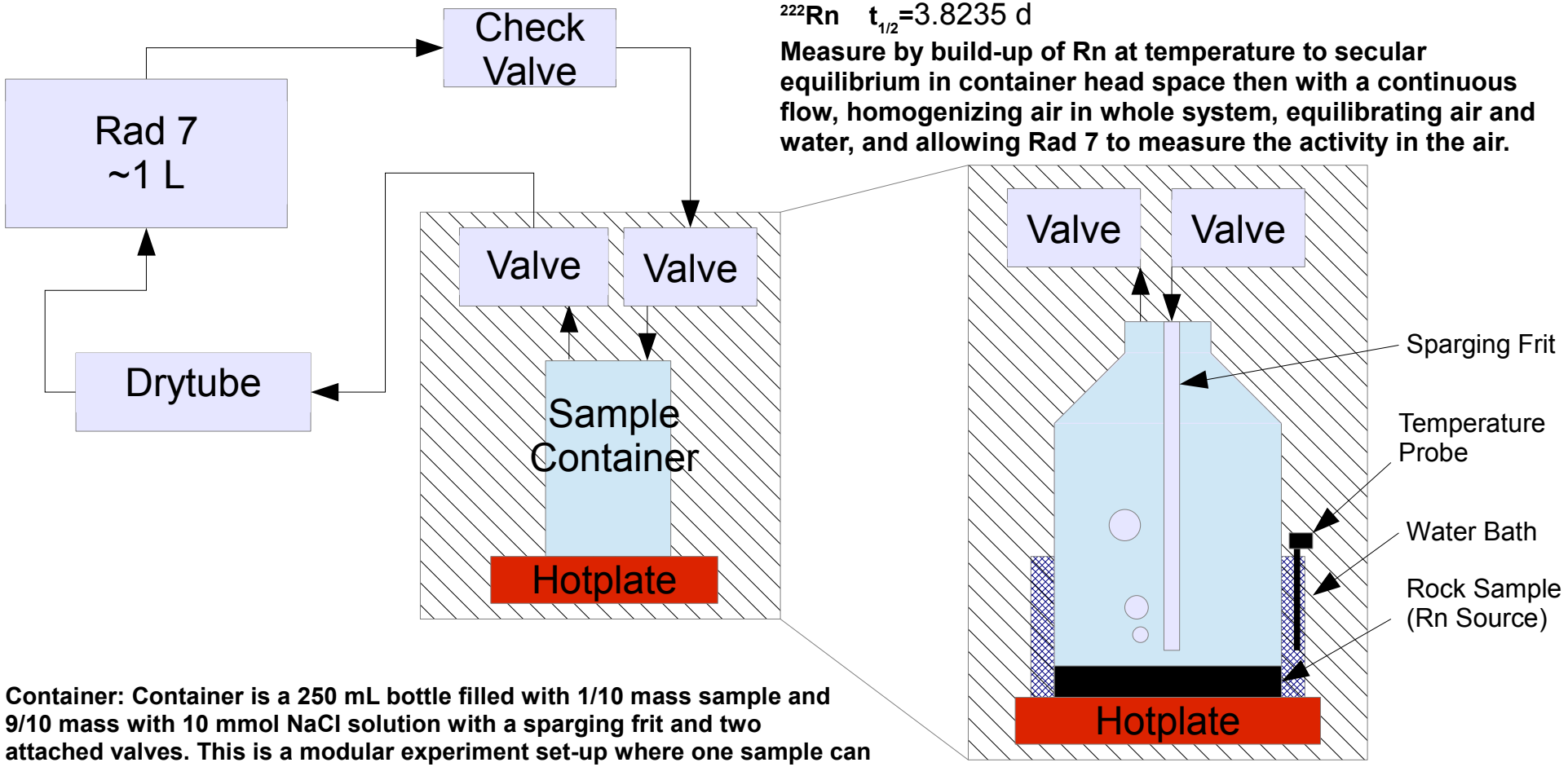

Container: Container is a 250 mL bottle filled with 1/10 mass sample and 9/10 mass with 10 mmol NaCl solution with a sparging frit and two attached valves. This is a modular experiment set-up where one sample can be switched out for another once the analysis is complete. This also allows for all samples to be building up Rn equilibrium at the same time which takes 20 days. Sample bottles will be placed in a water bath at their respective temperatures during the 20 day build up period and during the Rn analysis.

Arrows represent direction of flow.

System is in a closed loop making a closed system with a constant volume allowing for Rn to achieve secular equilibrium between an in-growth due to recoil and decay. Rn is measured in pCi/L in the air and then corrected for volume to get total activity of Rn in air.

The Rad7 pump will be run for 20 minutes to ensure the air is in equilibrium with the water. The Rad7 will measure ^{222}Rn for 36 cycles with each cycle lasting for 20 minutes. The air is pumped for 5 minutes at the beginning of the cycle then a single parcel of air is measured for an accurate ^{222}Rn activity.

Figure 1

Sample in Water Experiment for ^{220}Rn

Measuring:
One Grain Size (45-75 µm)
Three temperatures (21°C , 50° C and 90° C)
^{220}Rn $t_{1/2}$=55.6 s
Measure by build-up of Rn at temperature to secular equilibrium in container head space then with a continuous flow, homogenizing air in whole system, equilibrating air and water, and allowing Rad 7 to measure the activity in the air.

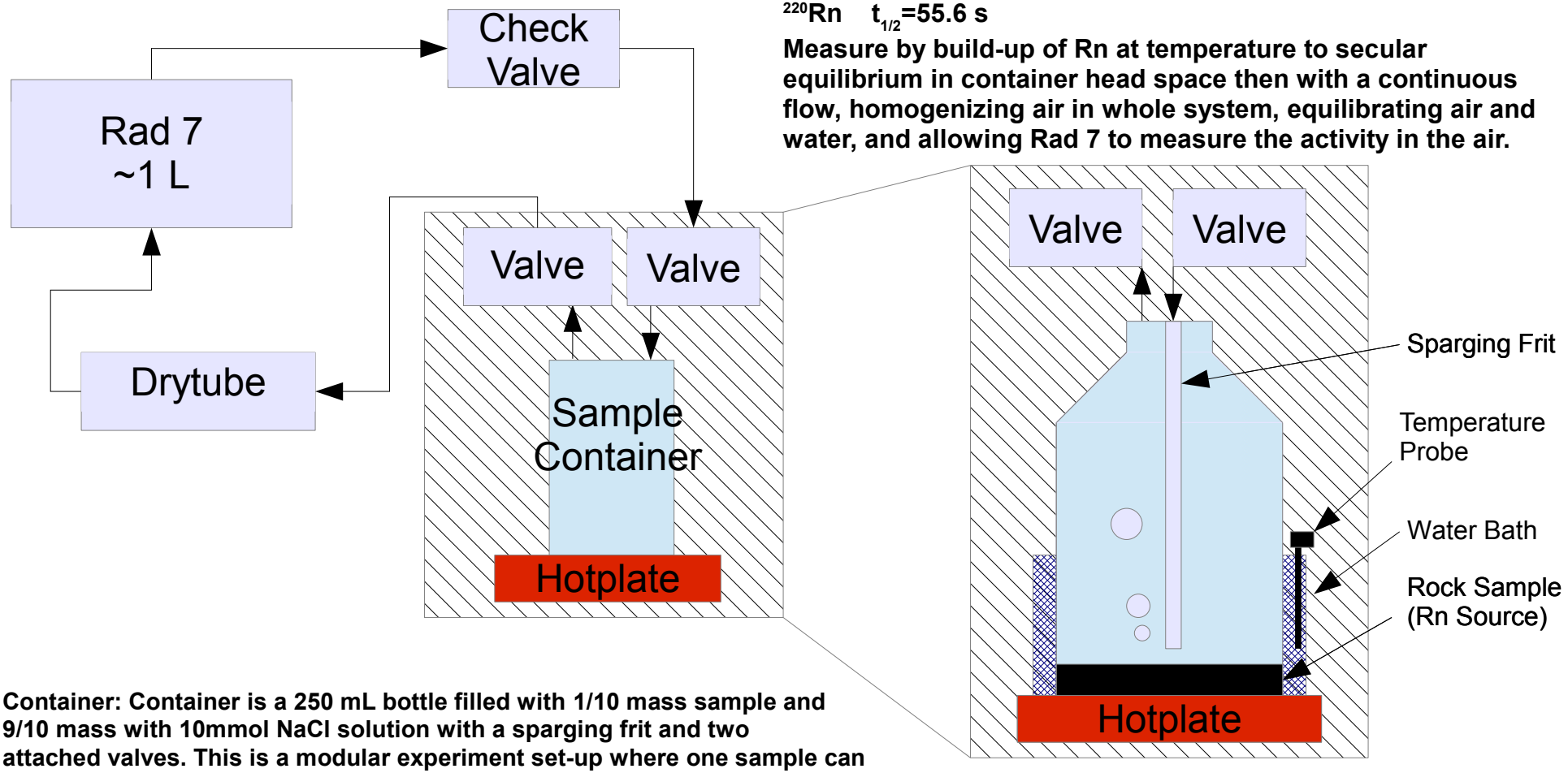

Container: Container is a 250 mL bottle filled with 1/10 mass sample and 9/10 mass with 10mmol NaCl solution with a sparging frit and two attached valves. This is a modular experiment set-up where one sample can be switched out for another once the analysis is complete. This also allows for all samples to be building up Rn equilibrium at the same time (20 days for ^{222}Rn).
Sample Bottles will be placed in a water bath at their respective temperatures during the 20 day build up period and during the Rn analysis.

Arrows represent direction of flow.

System is in a closed loop making a closed system with a constant volume allowing for Rn to achieve secular equilibrium between an in-growth due to recoil and decay.
Rn is measured in pCi/L in the air and then corrected for volume to get total activity of Rn in air.

Rad7 will measure ^{220}Rn for 36 cycles with each cycle lasting for 20 minutes. The air is pumped continuously through the whole run due to the short half life of ^{220}Rn.

APPENDIX B – MAP OF TRANSECTS FOR RN AND CO_2 SOIL FLUX OVER A NATURAL CO_2 RESERVOIR.

REPRODUCED FROM QUARTERLY PROGRESS REPORT FOR OCTOBER-DECEMBER 2011.

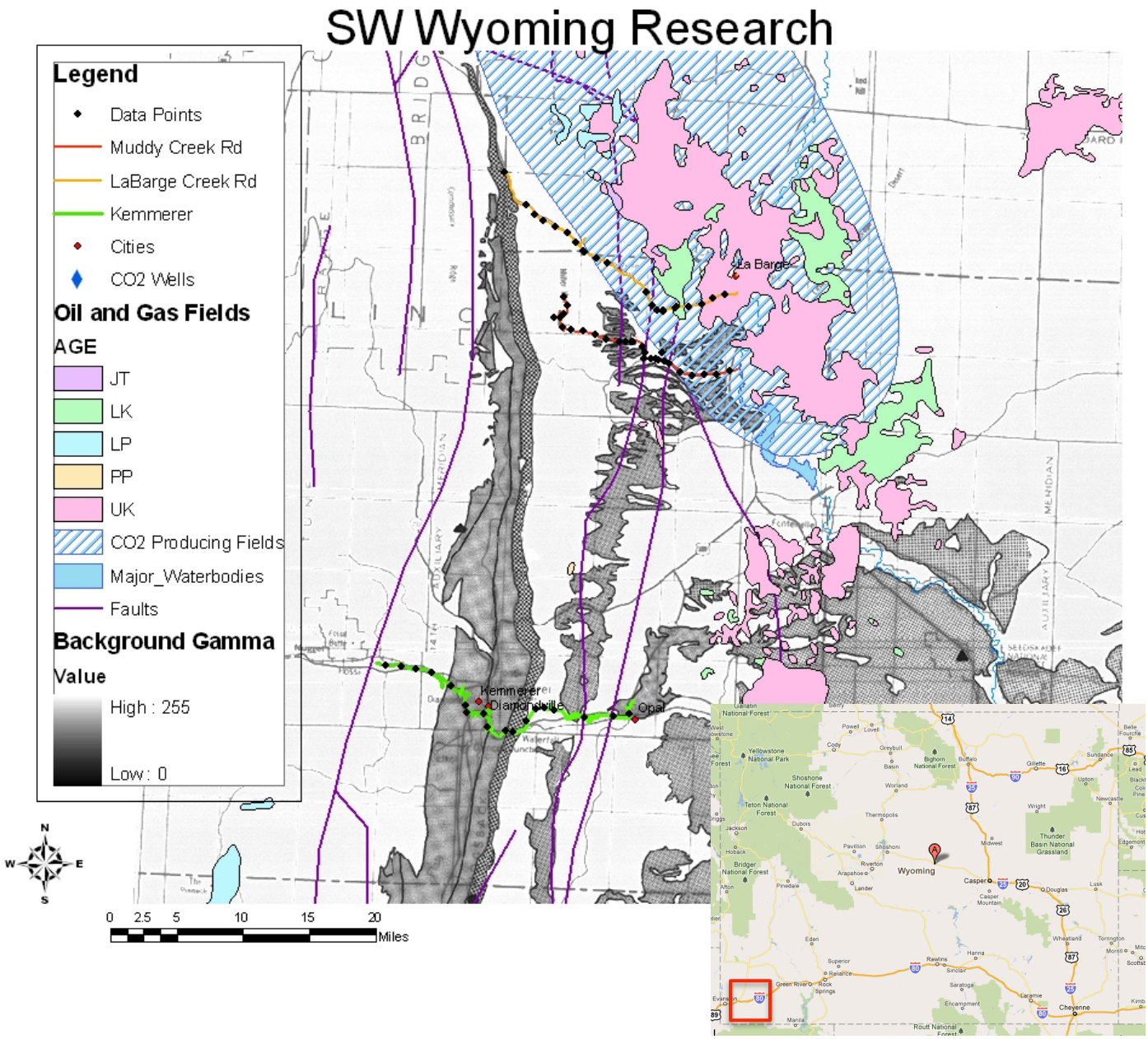

Map of study area and surrounding region. The insert in the bottom left of Wyoming shows where the GIS map is located boarded in a red box. The red line on the GIS map represents the Muddy Creek Road transect, the orange line represents the LaBarge Creek Road transect, and the green line represents the Kemmerer transect. The black points are GPS data points collected in each location a sample was taken. The data was taken approximately one mile apart with higher intensity in regions of interest, and blank areas in inaccessible regions. The solid purples line indicate faults, the gray represents different levels of background gamma radiation, the striped blue circle the water-gas contact of the LaBarge CO_2 Field, and the Oil and gas fields represented in color by age.

APPENDIX C – DATA FOR EXPERIMENTS EVALUATING SURFACE AREA, SURFACE:VOLUME RATIOS, AND LITHOLOGY

REPRODUCED FROM QUARTERLY PROGRESS REPORT FOR OCTOBER-DECEMBER, 2013.

Summary of Ambient Air Experiment Trial 1

			RAD7 readings						Emmision Coefficients						Ratio Comparison	
Rock Type	Grain Size	Mass (g)	^{222}Rn Solo (pCi/L)	± ^{222}Rn Solo (pCi/L)	^{222}Rn (pCi/L)	± ^{222}Rn (pCi/L)	^{220}Rn (pCi/L)	± ^{220}Rn (pCi/L)	^{222}Rn Solo (%)	± ^{222}Rn Solo (%)	^{222}Rn (%)	± ^{222}Rn (%)	^{220}Rn (%)	± ^{220}Rn (%)	^{220}Rn/^{222}Rn Calculated	^{220}Rn/^{222}Rn Measured
Banco Bonito Obsidian	4-6 mm	407.62	0.905	0.12	0.916	0.16	0.798	0.21	0.19%	0.03%	0.19%	0.03%	0.13%	0.03%	1.33	0.88
Banco Bonito Obsidian	0.85-1 mm	425.73	0.879	0.11	1.02	0.17	0.68	0.19	0.17%	0.02%	0.20%	0.04%	0.10%	0.03%	1.33	0.77
Banco Bonito Obsidian	45-75 µm	389.16	1.52	0.15	1.45	0.2	1.84	0.31	0.33%	0.04%	0.32%	0.05%	0.30%	0.05%	1.33	1.21
Guaje Pumice	4-6 mm	191.93	4.47	0.26	3.78	0.32	11.8	0.8	1.01%	0.08%	0.85%	0.08%	2.39%	0.20%	1.11	2.64
Guaje Pumice	0.85-1 mm	143.94	4.53	0.26	3.99	0.33	16.6	0.9	1.38%	0.11%	1.22%	0.12%	4.54%	0.34%	1.11	3.66
Guaje Pumice	45-75 µm	229.23	9.79	0.39	8.83	0.5	21.1	1.1	1.83%	0.12%	1.65%	0.13%	3.55%	0.26%	1.11	2.16
Cerros Del Rio Basalt	4-6 mm	423.7	15.8	0.5	14.1	0.6	5.85	0.57	25.24%	1.49%	22.52%	1.48%	10.24%	1.12%	0.91	0.37
Cerros Del Rio Basalt	0.85-1 mm	396.31	17.5	0.5	15.1	0.6	8.37	0.7	30.08%	1.73%	25.96%	1.66%	15.77%	1.54%	0.91	0.48
Cerros Del Rio Basalt	45-75 µm	292.57	17.3	0.5	15.7	0.7	9.13	0.7	41.27%	2.38%	37.45%	2.51%	23.88%	2.19%	0.91	0.53

Summary of Ambient Air Experiment Trial 2a

			RAD7 readings						Emmision Coefficients						Ratio Comparison	
Rock Type	Grain Size	Mass (g)	^{222}Rn Solo (pCi/L)	± ^{222}Rn Solo (pCi/L)	^{222}Rn (pCi/L)	± ^{222}Rn (pCi/L)	^{220}Rn (pCi/L)	± ^{220}Rn (pCi/L)	^{222}Rn Solo (%)	± ^{222}Rn Solo (%)	^{222}Rn (%)	± ^{222}Rn (%)	^{220}Rn (%)	± ^{220}Rn (%)	^{220}Rn/^{222}Rn Calculated	^{220}Rn/^{222}Rn Measured
Banco Bonito Obsidian	4-6 mm	407.62	2.04	0.17	2.22	0.24	0.667	0.19	0.43%	0.04%	0.46%	0.06%	0.10%	0.03%	1.33	0.33
Banco Bonito Obsidian	0.85-1 mm	425.73	1.86	0.17	1.86	0.23	0.77	0.21	0.37%	0.04%	0.37%	0.05%	0.12%	0.03%	1.33	0.41
Banco Bonito Obsidian	45-75 µm	389.16	6.73	0.33	2.55	0.27	1.37	0.28	1.48%	0.10%	0.56%	0.07%	0.23%	0.05%	1.33	0.20
Guaje Pumice	4-6 mm	191.93	6.48	0.31	4.93	0.36	10.4	0.7	1.49%	0.10%	1.11%	0.10%	2.11%	0.18%	1.11	1.60
Guaje Pumice	0.85-1 mm	143.94	5.89	0.29	5.6	0.38	14.8	0.9	1.80%	0.13%	1.71%	0.14%	4.05%	0.32%	1.11	2.51
Guaje Pumice	45-75 µm	229.23	9.74	0.39	7.91	0.47	12.7	0.8	1.83%	0.12%	1.48%	0.12%	2.14%	0.17%	1.11	1.30
Cerros Del Rio Basalt	4-6 mm	423.7	15.7	0.5	13.4	0.6	5.67	0.56	25.10%	1.49%	21.42%	1.44%	9.94%	1.10%	0.91	0.36
Cerros Del Rio Basalt	0.85-1 mm	396.31	17.3	0.5	15.2	0.7	5.46	0.55	29.75%	1.72%	26.14%	1.78%	10.29%	1.16%	0.91	0.32
Cerros Del Rio Basalt	45-75 µm	292.57	19.8	0.5	17.8	0.7	4.41	0.48	47.25%	2.65%	42.48%	2.70%	11.54%	1.38%	0.91	0.22

Summary of Ambient Air Experiment Trial 2b

			RAD7 readings						Emmision Coefficients						Ratio Comparison	
Rock Type	Grain Size	Mass (g)	^{222}Rn Solo (pCi/L)	± ^{222}Rn Solo (pCi/L)	^{222}Rn (pCi/L)	± ^{222}Rn (pCi/L)	^{220}Rn (pCi/L)	± ^{220}Rn (pCi/L)	^{222}Rn Solo (%)	± ^{222}Rn Solo (%)	^{222}Rn (%)	± ^{222}Rn (%)	^{220}Rn (%)	± ^{220}Rn (%)	^{220}Rn/^{222}Rn Calculated	^{220}Rn/^{222}Rn Measured
Banco Bonito Obsidian	4-6 mm	407.62	2.2	0.18	2.05	0.23	0.485	0.17	0.46%	0.04%	0.43%	0.05%	0.08%	0.03%	1.33	0.22
Banco Bonito Obsidian	0.85-1 mm	425.73	1.97	0.17	1.85	0.23	0.84	0.22	0.39%	0.04%	0.37%	0.05%	0.13%	0.03%	1.33	0.43
Banco Bonito Obsidian	45-75 µm	389.16	2.56	0.2	2.44	0.26	1.26	0.27	0.56%	0.05%	0.54%	0.06%	0.21%	0.05%	1.33	0.49
Guaje Pumice	4-6 mm	191.93	4.82	0.27	4.76	0.36	8.94	0.7	1.09%	0.08%	1.08%	0.10%	1.81%	0.17%	1.11	1.85
Guaje Pumice	0.85-1 mm	143.94	5.62	0.29	4.94	0.35	13.3	0.8	1.71%	0.12%	1.51%	0.13%	3.64%	0.28%	1.11	2.37
Guaje Pumice	45-75 µm	229.23	6.73	0.32	6.85	0.44	10.8	0.8	1.27%	0.09%	1.28%	0.10%	1.82%	0.16%	1.11	1.60
Cerros Del Rio Basalt	4-6 mm	423.7	12.5	0.5	12.4	0.6	6.76	0.6	19.97%	1.28%	19.81%	1.38%	11.84%	1.21%	0.91	0.54
Cerros Del Rio Basalt	0.85-1 mm	396.31	15.8	0.5	14.7	0.6	5.58	0.56	27.17%	1.61%	25.28%	1.63%	10.52%	1.18%	0.91	0.35
Cerros Del Rio Basalt	45-75 µm	292.57	16.6	0.5	16.2	0.7	4.2	0.47	39.61%	2.31%	38.66%	2.55%	10.99%	1.35%	0.91	0.25

Summary of Ambient Air Experiment Trial 2c

			RAD7 readings						Emmision Coefficients						Ratio Comparison	
Rock Type	Grain Size	Mass (g)	^{222}Rn Solo (pCi/L)	± ^{222}Rn Solo (pCi/L)	^{222}Rn (pCi/L)	± ^{222}Rn (pCi/L)	^{220}Rn (pCi/L)	± ^{220}Rn (pCi/L)	^{222}Rn Solo (%)	± ^{222}Rn Solo (%)	^{222}Rn (%)	± ^{222}Rn (%)	^{220}Rn (%)	± ^{220}Rn (%)	^{220}Rn/^{222}Rn Calculated	^{220}Rn/^{222}Rn Measured
Banco Bonito Obsidian	4-6 mm	407.62	1.77	0.16	1.23	0.18	0.706	0.19	0.37%	0.04%	0.26%	0.04%	0.11%	0.03%	1.33	0.40
Banco Bonito Obsidian	0.85-1 mm	425.73	1.75	0.16	1.23	0.18	0.7	0.2	0.35%	0.04%	0.24%	0.04%	0.10%	0.03%	1.33	0.40
Banco Bonito Obsidian	45-75 µm	389.16	2.55	0.2	2.33	0.25	1.48	0.29	0.56%	0.05%	0.51%	0.06%	0.24%	0.05%	1.33	0.58
Guaje Pumice	4-6 mm	191.93	4.62	0.26	4.49	0.35	8.54	0.7	1.04%	0.08%	1.01%	0.09%	1.73%	0.17%	1.11	1.85
Guaje Pumice	0.85-1 mm	143.94	5.41	0.28	5.19	0.39	13.6	0.8	1.65%	0.12%	1.58%	0.14%	3.72%	0.29%	1.11	2.51
Guaje Pumice	45-75 µm	229.23	6.69	0.32	6.73	0.32			1.25%	0.09%	1.26%	0.09%				
Cerros Del Rio Basalt	4-6 mm	423.7	13.4	0.5	12.7	0.6	5.31	0.55	21.42%	1.34%	20.31%	1.40%	9.31%	1.07%	0.91	0.40
Cerros Del Rio Basalt	0.85-1 mm	396.31	17.3	0.5	14.6	0.6	5.08	0.53	29.75%	1.72%	25.11%	1.63%	9.58%	1.11%	0.91	0.29
Cerros Del Rio Basalt	45-75 µm	292.57	15.4	0.5	15	0.6	3.51	0.43	36.75%	2.19%	35.80%	2.29%	9.18%	1.22%	0.91	0.23

Table 1: Data for experiments evaluating surface area, surface:volume ratios, and lithology. RAD7 readings show the average values after a 12 hour run. The ^{222}Rn Solo column is the data from the 20 minute pumping interval runs where ^{222}Rn and ^{220}Rn columns are the data from the continuous pumping runs. Emission Coefficients are calculated starting with the RAD7 Readings. Ratio comparison compares the calculated ^{220}Rn/^{222}Rn activity ratios based off of the literature with

Figure 1: Graphs of Radon and Thoron Emissivity versus grain size (decreasing to the right) for the Banco Bonito Obsidian. BBO T1 signifies the single run after a 20 day equilibration. BBO T2a-c signify the triple run after a 20 day equilibration.

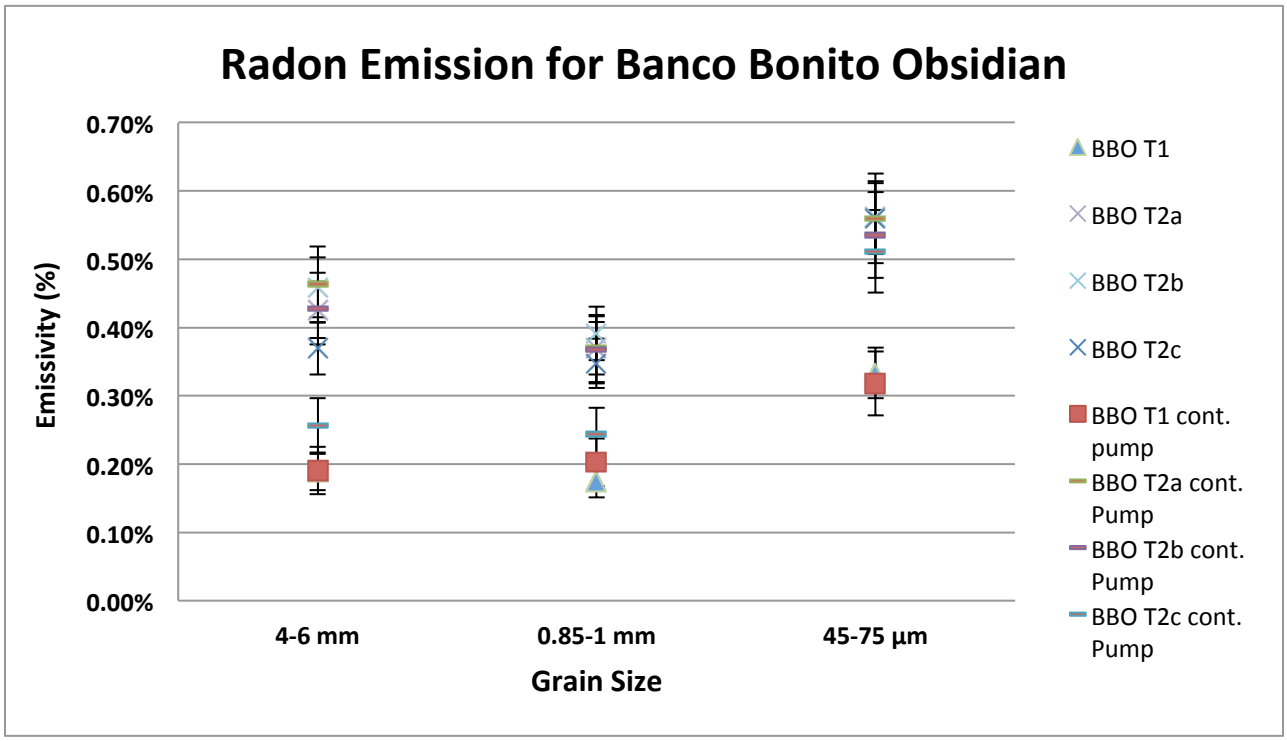

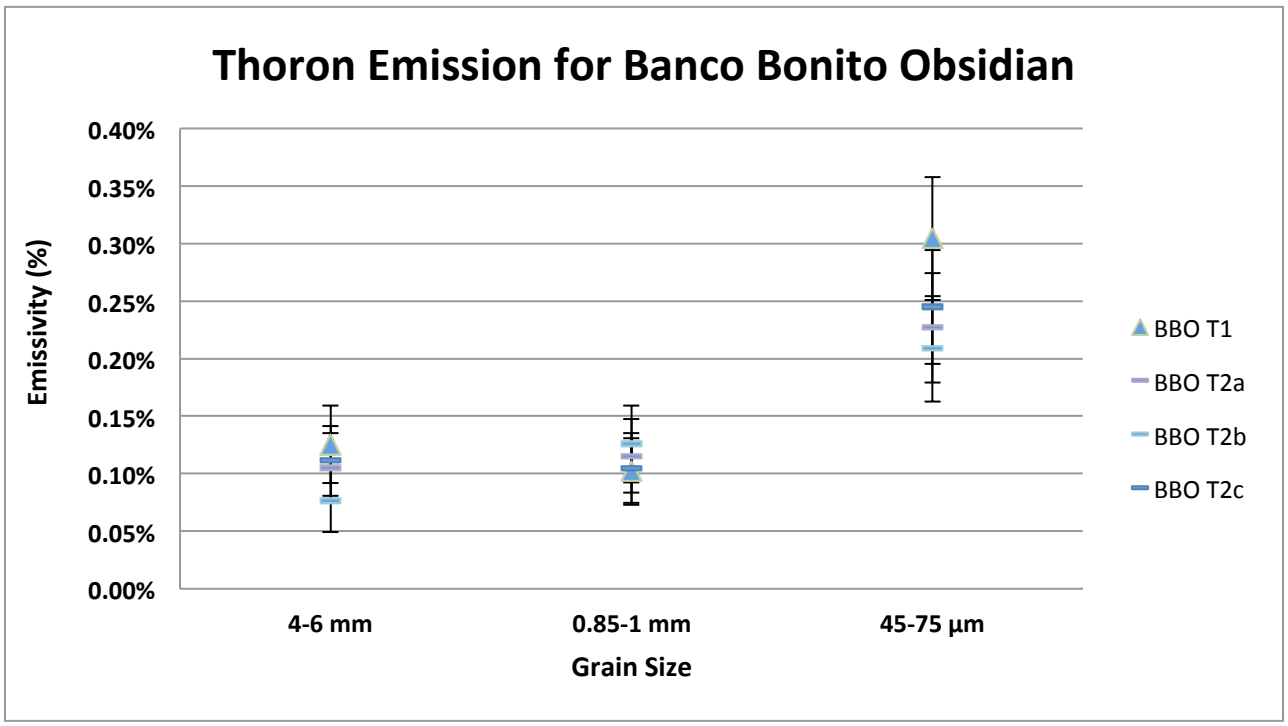

Figure 2: Graphs of Radon and Thoron Emissivity versus grain size (decreasing to the right) for the Cerros Del Rio Basalt. CDRB T1 signifies the single run after a 20 day equilibration. CDRB T2a-c signify the triple run after a 20 day equilibration.

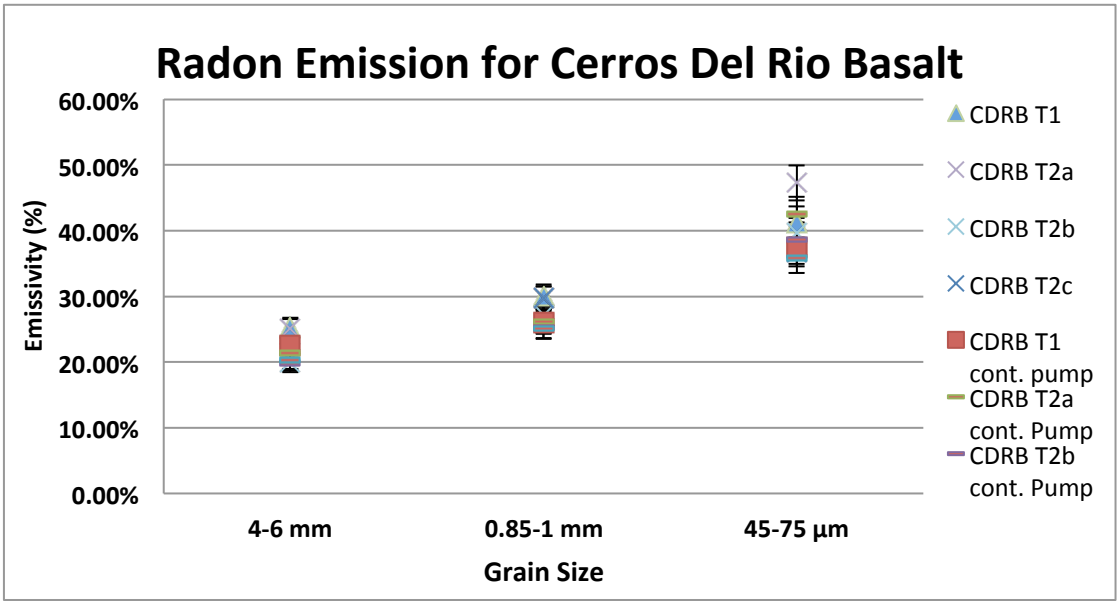

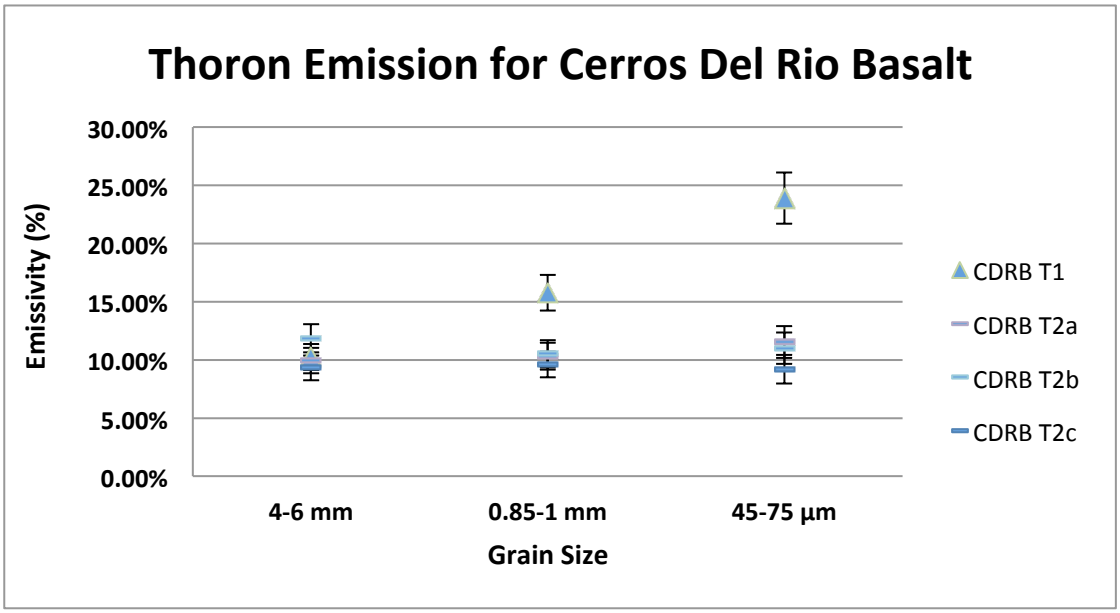

Figure 3: Graphs of Radon and Thoron Emissivity versus grain size (decreasing to the right) for the Guaje Pumice. GP T1 signifies the single run after a 20 day equilibration. GP T2a-c signify the triple run after a 20 day equilibration.

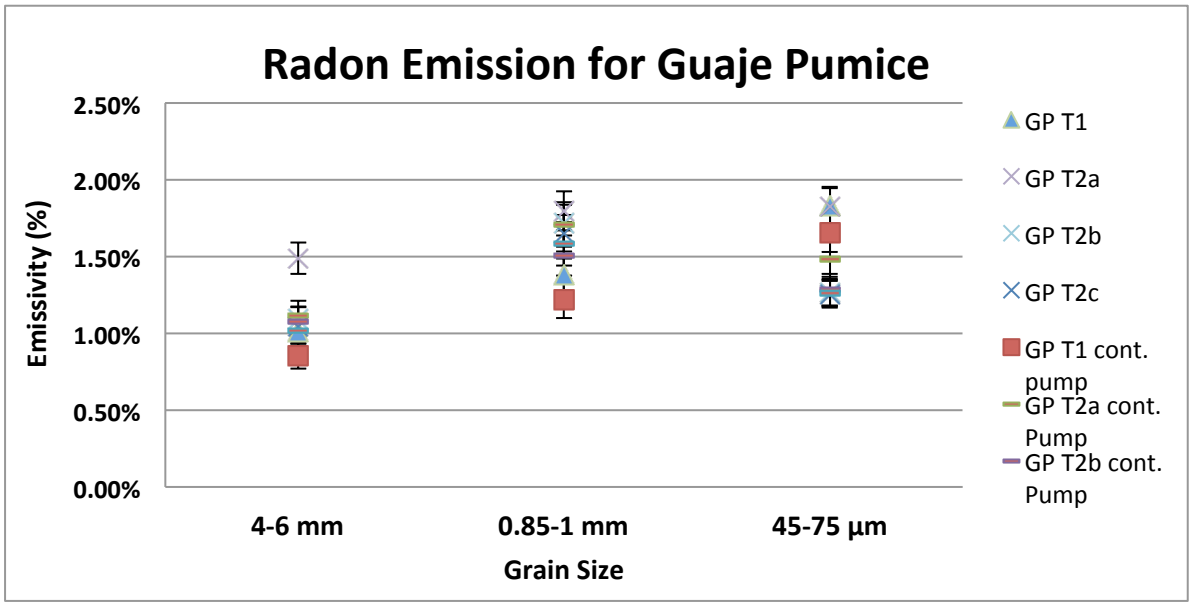

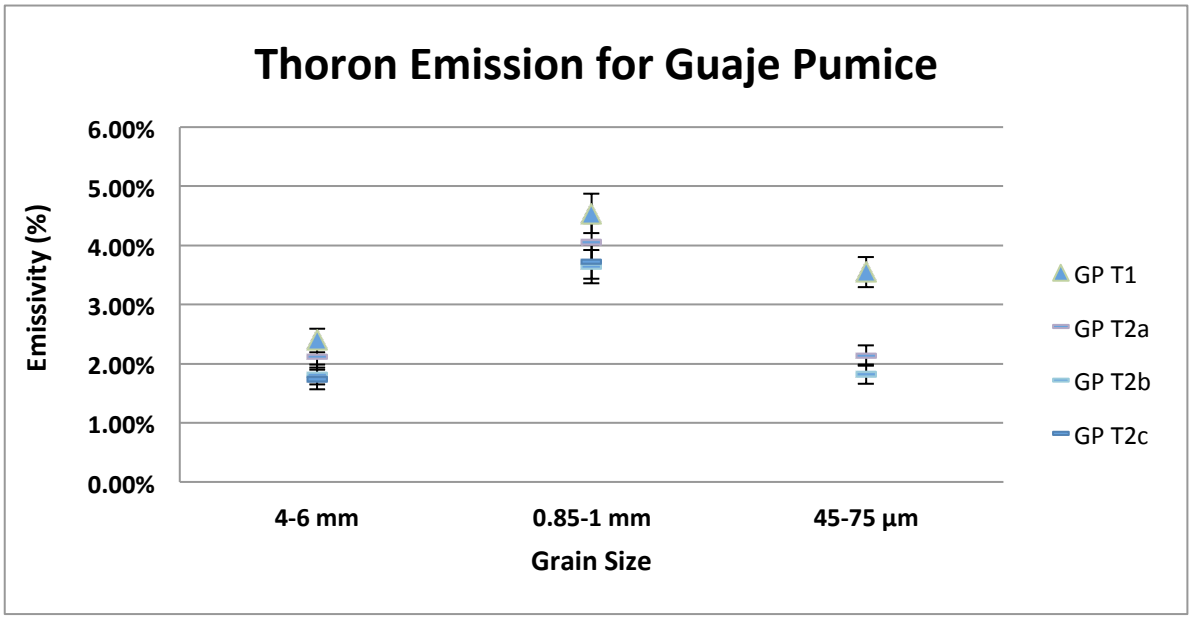

APPENDIX D - DATA FOR EXPERIMENTS EVALUATING REACTION OF SOURCE ROCK WITH FORMATION WATERS AND CO_2

THIS ORIGINAL DATASET WAS NOT PREVIOUSLY REPORTED.

Sample Activity (pCi/L)					
Experiment	**Temperature**	^{222}Rn cont pump	±^{222}Rn cont pump	^{220}Rn cont pump	±^{220}Rn cont pump
CDRH2OCO2-01	25 °C	4.67	0.34	0.65	0.20
CDRH2OCO2-02	40 °C	2.98	0.25	0.40	0.14
CDRH2OCO2-03	60 °C	4.74	0.37	0.90	0.24

Total Activity in Air (pCi)					
Experiment	**Temperature**	^{222}Rn cont pump	±^{222}Rn cont pump	^{220}Rn cont pump	±^{220}Rn cont pump
CDRH2OCO2-01	25 °C	4.74	0.42	0.66	0.21
CDRH2OCO2-02	40 °C	4.73	0.46	0.63	0.22
CDRH2OCO2-03	60 °C	7.52	0.70	1.43	0.39

Total Activity in Water (pCi)					
Experiment	**Temperature**	^{222}Rn cont pump	±^{222}Rn cont pump	^{220}Rn cont pump	±^{220}Rn cont pump
CDRH2OCO2-01	25 °C	0.23	0.02	0.03	0.01
CDRH2OCO2-02	40 °C	0.11	0.01	0.01	0.01
CDRH2OCO2-03	60 °C	0.13	0.01	0.03	0.01

Total Activity of System (pCi)					
Experiment	**Temperature**	^{222}Rn cont pump	±^{222}Rn cont pump	^{220}Rn cont pump	±^{220}Rn cont pump
CDRH2OCO2-01	25 °C	4.97	0.44	0.69	0.22
CDRH2OCO2-02	40 °C	4.83	0.47	0.65	0.23
CDRH2OCO2-03	60 °C	7.65	0.71	1.46	0.39

Emission Coefficient (%)					
Experiment	**Temperature**	^{222}Rn cont pump	±^{222}Rn cont pump	^{220}Rn cont pump	±^{220}Rn cont pump
CDRH2OCO2-01	25 °C	91.89%	8.05%	13.94%	4.37%
CDRH2OCO2-02	40 °C	89.28%	8.69%	13.14%	4.64%
CDRH2OCO2-03	60 °C	141.50%	13.08%	29.52%	7.99%

Table 2. Experimental data for CO_2-water-rock experiments. Sample Activity is the average of the RAD7 measurement after the 12 hour run.

Sample Activity (pCi/L)							
Experiment	**Temperature**	^{222}Rn 4m pump	±^{222}Rn 4m pump	^{222}Rn cont pump	±^{222}Rn cont pump	^{220}Rn cont pump	±^{220}Rn cont pump
CDRH2O-01	25 °C	0.63	0.08	1.16	0.12	0.50	0.14
CDRH2O-02	40 °C	0.53	0.08	1.41	0.14	0.42	0.16
CDRH2O-03	60 °C	1.65	0.16	2.11	0.18	0.76	0.20
CDRH2O-11	25 °C	N/A	N/A	2.58	0.23	0.38	0.13
CDRH2O-12	40 °C	N/A	N/A	1.90	0.18	0.23	0.09
CDRH2O-13	60 °C	N/A	N/A	2.67	0.26	0.48	0.16

Total Activity in Air (pCi)							
Experiment	**Temperature**	^{222}Rn 4m pump	±^{222}Rn 4m pump	^{222}Rn cont pump	±^{222}Rn cont pump	^{220}Rn cont pump	±^{220}Rn cont pump
CDRH2O-01	25 °C	0.64	0.09	1.18	0.14	0.51	0.15
CDRH2O-02	40 °C	0.84	0.13	2.24	0.25	0.67	0.26
CDRH2O-03	60 °C	2.62	0.29	3.35	0.33	1.21	0.32
CDRH2O-11	25 °C	N/A	N/A	2.61	0.27	0.38	0.13
CDRH2O-12	40 °C	N/A	N/A	3.00	0.32	0.36	0.14
CDRH2O-13	60 °C	N/A	N/A	4.23	0.46	0.76	0.26

Total Activity in Water (pCi)							
Experiment	**Temperature**	^{222}Rn 4m pump	±^{222}Rn 4m pump	^{222}Rn cont pump	±^{222}Rn cont pump	^{220}Rn cont pump	±^{220}Rn cont pump
CDRH2O-01	25 °C	0.03	0.00	0.06	0.01	0.02	0.01
CDRH2O-02	40 °C	0.02	0.00	0.05	0.01	0.02	0.01
CDRH2O-03	60 °C	0.05	0.00	0.06	0.01	0.02	0.01
CDRH2O-11	25 °C	N/A	N/A	0.13	0.01	0.02	0.01
CDRH2O-12	40 °C	N/A	N/A	0.07	0.01	0.01	0.00
CDRH2O-13	60 °C	N/A	N/A	0.08	0.01	0.01	0.00

Total Activity of System (pCi)							
Experiment	**Temperature**	^{222}Rn 4m pump	±^{222}Rn 4m pump	^{222}Rn cont pump	±^{222}Rn cont pump	^{220}Rn cont pump	±^{220}Rn cont pump
CDRH2O-01	25 °C	0.68	0.09	1.24	0.14	0.53	0.15
CDRH2O-02	40 °C	0.86	0.14	2.29	0.25	0.69	0.26
CDRH2O-03	60 °C	2.67	0.29	3.41	0.34	1.23	0.33
CDRH2O-11	25 °C	N/A	N/A	2.74	0.28	0.40	0.14
CDRH2O-12	40 °C	N/A	N/A	3.07	0.33	0.37	0.15
CDRH2O-13	60 °C	N/A	N/A	4.30	0.47	0.77	0.26

Emission Coefficient (%)							
Experiment	**Temperature**	^{222}Rn 4m pump	±^{222}Rn 4m pump	^{222}Rn cont pump	±^{222}Rn cont pump	^{220}Rn cont pump	±^{220}Rn cont pump
CDRH2O-01	25 °C	12.50%	1.70%	22.94%	2.62%	10.82%	3.08%
CDRH2O-02	40 °C	15.93%	2.53%	42.30%	4.69%	13.88%	5.31%
CDRH2O-03	60 °C	49.42%	5.38%	63.20%	6.23%	24.92%	6.68%
CDRH2O-11	25 °C	N/A	N/A	50.62%	5.14%	8.17%	2.82%
CDRH2O-12	40 °C	N/A	N/A	56.75%	6.06%	7.43%	2.97%
CDRH2O-13	60 °C	N/A	N/A	79.41%	8.68%	15.62%	5.27%

Table 1. Experimental data for water-rock experiments. Sample Activity is the average of the RAD7 measurement after the 12 hour run.